Supporting Information for:

Multiphase chemistry controls inorganic chlorinated and nitrogenated compounds in indoor air during bleach cleaning

James M. Mattila[1], Pascale S. J. Lakey[2], Manabu Shiraiwa[2], Chen Wang[3], Jonathan P.D. Abbatt[3], Caleb Arata[4,5], Allen H. Goldstein[5,6], Laura Ampollini[7], Erin F. Katz[8], Peter F. DeCarlo[7,8], Shan Zhou[9], Tara F. Kahan[9,10], Felipe J. Cardoso-Saldaña[11], Lea Hildebrandt Ruiz[11], Andrew Abeleira[1], Erin K. Boedicker[1], Marina E. Vance[12], Delphine K. Farmer[1]*

[1]Department of Chemistry, Colorado State University, Fort Collins, Colorado 80523, United States

[2]Department of Chemistry, University of California, Irvine, California 92697, United States

[3]Department of Chemistry, University of Toronto, Toronto, ON Canada M5S 3H6

[4]Department of Chemistry, University of California, Berkeley, California 94720, United States

[5]Department of Environmental Science, Policy, and Management, University of California, Berkeley, California 94720, United States

[6]Department of Civil and Environmental Engineering, University of California, Berkeley, California 94720, United States

[7]Department of Civil, Architectural, and Environmental Engineering, Drexel University, Philadelphia, Pennsylvania 19104, United States

[8]Department of Chemistry, Drexel University, Philadelphia, Pennsylvania 19104, United States

[9]Department of Chemistry, Syracuse University, Syracuse, New York 13244, United States

[10]Department of Chemistry, University of Saskatchewan, Saskatoon, SK Canada S7N 5C9

[11]Center for Energy and Environmental Resources, The University of Texas at Austin, Austin, Texas 78758, United States

[12]Department of Mechanical Engineering, University of Colorado Boulder, Boulder, Colorado 80309, United States

**Correspondence to:* Delphine K. Farmer (Delphine.Farmer@colostate.edu)

No. of pages: 36

No. of figures: 15

No. of tables: 7

Supporting Information Text

Section S1: Detailed kinetic model description including assumptions and simplifications. The building interior has a volume of 250 m^3 and the bleached surface area was 40 m^2. In the model, we assume that the bleach thickness was 0.01 cm. We did not treat changes in the bleach thickness over time as the thickness was unmeasured and the rate of evaporation was unknown. Bleach contains ~6% NaOCl by mass. The bleach had been diluted by a factor of 32 before being applied to the floor. The model considers an initial concentration of aqueous OCl^- of 1.5×10^{19} molecules cm^{-3}. The pH of the bleach was varied in the model until the gas-phase HOCl and Cl_2O data were well fit. This approach resulted in a pH range of 9.2 – 9.6. These values are reasonable considering the bleach pH of ~12.6 and a dilution factor of 32 with possible further acidification by other molecules present on the floor. The pH was assumed to remain constant over time as changes were unmeasured. During the experiments, the bleach was applied throughout a period of 10 minutes. However, in the model, applying the bleach over this extended time period was challenging, and the best model-measurement agreement was obtained when the reactions were switched on ~2.5 minutes after bleach cleaning had started. After a set time (0.31 – 0.56 hours; determined by observations in measurement data), we assumed that the bleach had fully evaporated away and sorption and desorption from the bleach mixture in the model was switched off. Anything remaining in the bleach was then assumed to act as a residue on the floor.

Mass-transport across the boundary layer provides kinetic limitations for uptake into the bleach and was assumed to be influenced by eddy diffusion such that the gas-phase diffusion coefficient ($D_{h,Z}$) at a height, h, above a surface could be calculated as:

$$D_{h,Z} = D_{g,Z} + K_e \times h^2$$

where $D_{g,Z}$ is the gas-phase diffusion coefficient under non-turbulent conditions and K_e is the turbulence intensity. The values of $D_{g,Z}$ are listed in Table S3 while the values of K_e are listed in Table S4. Air exchange rates are also listed in Table S4 and were constrained by measurements described in Section S2.

We include photolysis rates (j) derived from solar irradiance measurements performed indoors during HOMEChem (section S2; Figure S7). These solar irradiance measurements were performed directly adjacent to windows in the house; resultant photolysis rates likely do not account for the spatial variability due to the inhomogeneous transmission of outdoor light to indoors. We therefore treat these measured photolysis rates as upper-limits, and accordingly tune these values in our model to match measurement observations. Sensitivity tests revealed that the photolysis rate of $ClNO_2$, NO_3 and HONO

were insensitive up to the maximum photolysis rate while the photolysis rate of Cl_2 and HOCl had to be at least a factor of 10 and 5 lower than the maximum value, respectively, in order to reproduce respective measurement data. The model results were still slightly sensitive to the NO_2 photolysis rate when the maximum value was decreased by a factor of 50. Modeled O_3 mixing ratios were very sensitive to indoor photolysis processes (e.g. reactions 8, 33, 35, and 41 in Table S2). The slight enhancements in measured indoor O_3 (measurement details in Farmer et al.[1]) are reproducible across bleach cleaning experiments, even during the evening in the absence of transmission of outdoor sunlight (20:35 on 10 June 2018; Figure S8). We therefore suspect these enhancements were not driven by photochemistry. NO reacts with ClO to produce NO_2 and Cl.[2, 3] However, we observe consistent decays in NO mixing ratios across bleach cleaning experiments, even in the absence of transmission of outdoor sunlight (20:35 on 10 June 2018; Figure S3 and S8). We therefore do not consider NO loss to be driven by photochemistry (i.e. loss via ClO is unlikely). We determined that measurement observations herein are best reproduced by decreasing upper-limit photolysis rates by a factor of 50. Photolysis rates used in the model are reported in Table S4.

Other unknown or uncertain parameters including some rate coefficients, losses to surfaces and uptake coefficients (see Table S4) were varied systematically and iteratively until the measurements could be reproduced. A surface mass accommodation of 1 and a desorption lifetime of 1 ns was assumed for all (semi)volatile species.

Section S2: Additional HOMEChem measurement details.

Air exchange rate.

We determine the air exchange rate (AER) of the test house via the monitoring of a continuously emitted inert tracer gas (butane-d3, Cambridge Isotope Laboratories) with a PTR-TOF-MS. This method is detailed in Liu et al.[4] AER values calculated during bleach cleaning experiments are in Table S4.

PTR-TOF-MS sensitivity estimation.

We estimate PTR-TOF-MS sensitivity toward NH_2Cl and $NHCl_2$ following Zhao and Zhang[5], and assuming a proton-transfer reaction rate of a typical VOC ($k = 2.5 \times 10^{-9}$ cm^3 s^{-1}). Typically, PTR-TOF-MS sensitivity errors for uncalibrated VOCs are around ± 50%. Given our limited information in constraining PTR-TOF-MS sensitivity toward NH_2Cl and $NHCl_2$, these errors could be larger. PTR-TOF-MS sensitivities can depend on humidity, and calibrations were conducted at 0% RH. Fluctuations in sensitivity due to indoor

RH should be negligible during this study given the low variability in the humidity of indoor air during the experiments (typically ± 2% RH).

Particulate matter surface area.

We determine particulate matter (PM) surface area with an Ultra High Sensitivity Aerosol Spectrometer (UHSAS; Droplet Measurement Technologies, Inc.) (Figure S1). The UHSAS sampled PM between 60 - 1000 nm through a copper sampling line (8 m length; 0.635 cm ID; 0.9525 cm OD), attached to a valve-switching system which included a HEPA bypass and a Nafion dryer. Additional details of these measurements at HOMEChem are found in Farmer et al.[1] We acknowledge that this submicron aerosol surface area is an underestimate of the total PM surface area during cooking events.

Indoor photolysis rates.

Wavelength-resolved spectra of sunlight entering the house were measured using an Ocean Optics USB4000 spectrometer attached with a 1 m fiber optic cable (Thorlabs) and a Spectralon cosine receptor. Photon fluxes (F) were estimated as being equal to the measured irradiance. This estimation is likely accurate under sunny conditions at low solar zenith angles (i.e. when sunlight entering the house is largely collimated and unidirectional), as discussed in Kowal et al.[6] Irradiance likely underestimates photon flux when sunlight is highly diffuse, such as on cloudy days. The average photon fluxes reported near the windows (shown in Figure 4 in the manuscript) are therefore likely underestimated by up to 25%. Photolysis rate constants (J) of HOCl, Cl_2, $ClNO_2$, NO_2, NO_3, and HONO were calculated (Figure S7; Table S2) as described previously using the measured photon fluxes (F) and reported absorption cross sections (σ) and photolysis quantum yields (ϕ):[6]

$$J = \int_{\lambda_i}^{\lambda_j} \sigma(\lambda)\phi(\lambda)F(\lambda)d\lambda$$

Continuous measurements were made directly adjacent to windows at 1-minute resolution. As a result, these rate constants represent local values. Indoor solar photon flux has been shown to decrease linearly with distance from windows and displayed high spatial heterogeneity.[1,6] We therefore treat these local photolysis rates as upper bounds. We note that the main function of these measurements was to characterize the indoor diel profile, rather than the absolute magnitudes, of photolysis rates, in that the magnitudes of these rates were tuned in our kinetic model to match indoor observations (see section S1). Additional details of these measurements during HOMEChem are found in Farmer et al.[1]

Kowal et al.[6] demonstrated that UV photon fluxes from indoor lighting fixtures decay very rapidly with distance. We therefore expect negligible photolysis due to indoor lighting during HOMEChem.

Additional AMS measurement details.

Cooking organic aerosol is largely comprised of molecules with lower oxidation states (e.g. oleic acid and other unsaturated fatty acids).[34] Xu et al.[35] reported an AMS relative ionization efficiency (RIE) of 2-7 for cooking organic aerosol. Organic PM mass concentration data reported in Figure S5 use RIE = 1.4, a value typical for ambient organic aerosols.[35] As a result, these organic PM mass concentrations during cooking events (e.g. Figure S5a-d) are likely overestimated. We use an RIE of 1.3 for AMS measurements of non-refractory particulate Cl^- during all experiments herein.

We provide additional I^- TOF-CIMS measurement details in the subsequent sections.

Section S3: I^- TOF-CIMS operation and data processing. Ultra-high purity (UHP) N_2 (Airgas) flowed (~0.7 L min^{-1}) through a heated oven (50 °C) containing methyl iodide (CH_3I) permeation tubes (VICI, Dynacalibrator). The resulting CH_3I-saturated N_2 stream passed through a ^{210}Po ionizer to generate I^- reagent ions, which then entered the ion-molecule reactor (IMR) region of the instrument. Here, analytes sampled from ambient air (M) form charged iodide-analyte adducts ($[I+M]^-$) via clustering reactions with I^-, or ligand switching reactions with IH_2O^-;[7, 8] followed by transmission via ion optics to the TOF region of the instrument for detection. We controlled mass spectral data acquisition with TofDaq Recorder (Tofwerk AG; extraction frequency = 26 kHz; m/z range = 1.63 – 456.80).

We processed I^- TOF-CIMS data in Igor Pro (WaveMetrics Inc., version 6) with Tofware (Tofwerk AG, Aerodyne Research Inc., version 2.5.10), which calculated mass spectral baseline, fitted peak shape, and mass resolution. Tofware uses the integrated area of fitted peak functions to mass spectral data to calculate signal time series of mass spectral peaks. The peak fitting algorithm featured in Tofware automatically calculates relative isotopic contributions of fitted peak functions based on the elemental assignment of a mass spectral peak. From this, we are able to confirm the elemental compositions of peaks in our TOF-CIMS spectra, including the chlorinated and nitrogenated compounds discussed herein. Mass calibration took place post-acquisition using a three-parameter fit to the NO_2^-, I^-, IH_2O^-, $ICH_2O_2^-$, $IC_3H_6O_3^-$, and I_3^- peaks. These peaks had consistently high resolution and contained no interferences nor

overlapping peaks throughout the campaign. TOF-CIMS mass accuracy was 4 ppm (campaign average of mass calibrant ions), and resolution (m/Δm) was > 4000. Tofware's high-resolution peak fitting algorithm extracted time series of mass spectral signal (Hz) for detected analytes. We performed additional data analysis, including background subtraction, normalization, and mixing ratio calculation/estimation in Igor Pro. We normalized measured analyte data to the total reagent ion signal following Bertram et al.[9], by multiplying mass spectral signal by the ratio of the average total reagent ion signal during an hourly background measurement to the total reagent ion signal during periods of analyte measurement. Here, we calculated total reagent ion signal as the sum of I^- and IH_2O^- signal. This normalization method ensured that any changes in analyte signal were not due to variations in total reagent ion signal. We calculated I^- TOF-CIMS instrumental detection limits for various bleach-related compounds measured at HOMEChem following Bertram et al. [9], and provide them in Table S5.

Section S4: Shared TOF-CIMS sampling inlet setup and on-site alkanoic acid calibrations at HOMEChem. Our I^- TOF-CIMS, and an acetate (Ac^-) TOF-CIMS shared a sampling inlet and calibration system, outlined in Figure S9. We deployed both TOF-CIMS instruments in a temperature-controlled trailer directly adjacent to the UTest house. We sampled ambient air from inside the house through perfluoroalkoxy alkane (PFA) tubing (0.3175 cm ID) extending from the kitchen area of the UTest house to inside the trailer at ~4 L min^{-1}. We also sampled outdoor air through PFA tubing (0.3175 cm ID), extending from roughly 1 m above the trailer to inside the trailer at ~4 L min^{-1}. These indoor and outdoor sampling lines met at the three-way solenoid isolation valve (NResearch Inc.). Total indoor and outdoor sampling inlet lengths were 7 m and 5 m, respectively, for the I^- TOF-CIMS; and 10 m and 8 m, respectively, for the Ac^- TOF-CIMS.

Ambient sampling typically followed an automated hourly indoor/outdoor switching cycle (Figure S10). At the start of each hour, we performed two-minute instrumental background measurements by introducing an overflow of ultra-zero grade air (UZA, Airgas) to both TOF-CIMS using a mass-flow controller (MFC). Indoor/outdoor ambient sampling comprised the remainder of the hourly cycle. We neglect data collected within 60 seconds of a valve-switching event to avoid the influence of potential sampling line effects. Sampled air entered the IMR of both TOF-CIMS at ~2 L min^{-1}. We performed inline measurements of ambient temperature and relative humidity (RH) using a digital sensor (Sensirion SHT21) controlled by an EyeOn control system (Aerodyne Research Inc.). We

automated valves, MFCs, and mass spectral data acquisition using homebuilt programs (LabVIEW, National Instruments).

We generated gas-phase calibration standards of formic (CH_2O_2), acetic ($C_2H_4O_2$), propionic ($C_3H_6O_2$), butyric ($C_4H_8O_2$), and valeric acid ($C_5H_{10}O_2$) by flowing ultra-high purity (UHP) N_2 (Airgas) through a heated oven (40 °C) containing permeation tubes (VICI, Dynacal) of each compound. We determined temperature-dependent mass losses gravimetrically, enabling us to calculate measured mixing ratios of each standard. We performed single-point hourly standard addition calibrations on 12-16, 18, 25, and 27 June by introducing gas-phase calibrant into the ambient sampling stream and measuring the signal change due to a known stepwise change in mixing ratio (Figure S9). Standard additions took place at nights between the hours of 21:00 and 05:00, i.e. in the absence of interferences from indoor experiments. Using a sufficiently small calibrant flow during standard additions (~0.1 L min^{-1}; 2.5% of total sample flow) ensured that any analyte dilution from this flow was negligible. We also performed five-point external standard calibrations of these compounds on 9, 14, 23, and 28 June by diluting gas-phase calibrant in UZA (Airgas) using an MFC (MKS Instruments) (Figure S9). All tubing used downstream of our calibration source was 0.3175 cm ID PFA.

Section S5: I^- TOF-CIMS calibrations for Cl_2, HOCl, N_2O_5, and $ClNO_2$. We performed in-laboratory I^- TOF-CIMS calibrations for Cl_2, HOCl, N_2O_5, and $ClNO_2$ shortly after the conclusion of the HOMEChem campaign. We detect all calibrant compounds as iodide-analyte adducts. We minimize lengths of Teflon tubing (PFA; 0.3175 cm ID) used in all calibration setups to mitigate any inlet-effects.

Cl_2 and HOCl calibrations.

We conducted five-point external standard calibrations for Cl_2 using a gas-phase standard (Airgas; 2 ppm Cl_2 in UHP N_2; 99.5% purity). We calibrated the instrument for HOCl based on the methodology of Foster et al.[10] and Lawler et al.[11]. Here, we flowed UHP N_2 (Airgas; ~100 sccm) over the headspace of a ~0.3 M NaOCl solution (RICCA; commercial grade), generating a steady flow of a gaseous mixture containing HOCl and Cl_2. This initial headspace flow entered the instrument inlet to measure HOCl and Cl_2 I^- TOF-CIMS response. We then redirected the headspace flow into a glass tube (2.5 cm OD) containing an aqueous slurry of NaCl (EMD Millipore; GR ACS) and HCl (EMD Millipore; GR ACS), converting HOCl to Cl_2.[10] We held the glass tube containing this slurry in an ice bath to inhibit volatilization of HCl. We

determined I^- TOF-CIMS sensitivity to HOCl from the measured increase in Cl_2 signal, and associated decrease in HOCl signal following this conversion. We calculated Cl_2 and HOCl I^- TOF-CIMS sensitivities of 4. ± 1. Hz $pptv^{-1}$ and 0.4 ± 0.2 Hz $pptv^{-1}$, respectively.

N_2O_5 calibration.

We flowed ~10 sccm UZA (Airgas) through a Hg lamp (UVP) to generate ozone (O_3), which reacted with ~15 sccm nitrogen dioxide (NO_2; Praxair, Inc.) gas to produce NO_3, which further reacted with NO_2 to generate a flow of gaseous N_2O_5. We determined mixing ratios of N_2O_5 produced via this process using a custom-built cavity ring-down spectroscopy (CRDS) instrument.[12-14] We directed the N_2O_5 standard to the I^- TOF-CIMS sampling inlet to determine instrumental sensitivity to $IN_2O_5^-$ and 'total N_2O_5' (taken as $IN_2O_5^- + NO_3^-$)[8] via five-point external standard calibrations. We calculated a total N_2O_5 I^- TOF-CIMS sensitivity of 50. ± 10. Hz $pptv^{-1}$.

$ClNO_2$ calibration.

We determined instrumental response to $ClNO_2$ via five-point external standard calibrations. Here, we flowed ~25 sccm gaseous N_2O_5 into a glass tube (2.5 cm OD) containing an aqueous NaCl (EMD Millipore; GR ACS) slurry, thereby converting N_2O_5 to $ClNO_2$.[15, 16] We determined <10% N_2O_5 formed HNO_3 as a side-product, based on our I^- TOF-CIMS sensitivity to HNO_3 determined via external standard calibration utilizing an HNO_3 permeation tube standard (KIN-TEK Analytical, Inc.). We calculated a $ClNO_2$ I^- TOF-CIMS sensitivity of 6. ± 3. Hz $pptv^{-1}$.

Accounting for dependence of I^- TOF-CIMS sensitivities on ambient humidity.

Water vapor present in the IMR region of the TOF-CIMS affects I^- TOF-CIMS sensitivities for several compounds. Ambient humidity was therefore as a potential matrix effect during our HOMEChem measurements. We accounted for this by performing our post-campaign calibrations (and associated instrumental background measurements) of Cl_2, HOCl, N_2O_5, and $ClNO_2$ with a dilution flow of humidified ultra zero grade air (UZA; Airgas). We flowed UZA through a glass bubbler containing LC-MS grade H_2O (EMD Millipore), generating a UZA flow saturated with H_2O. We controlled the final relative

humidity (RH) of this flow by mixing a second flow of UZA downstream of the bubbler, and measured its final RH using an in-line RH sensor (OMEGA Engineering, Inc; HX71-V1). Mass-flow controllers (MFCs; MKS) modulated UZA flow rates. We maintained a setpoint RH during calibrations with a proportional-integral-derivative (PID) loop using homebuilt software (LabVIEW; National Instruments) interfaced with the MFCs and RH sensor. The UZA dilution flows used for these calibrations/backgrounds were humidified such that the partial pressure of water vapor in the IMR ($P_{H2O,IMR}$) was comparable to that during ambient sampling at HOMEChem ($P_{H2O,IMR} \approx 1.4$ mbar, corresponding to ~55% RH measured in-line during HOMEChem).

Figure S11 shows how in-laboratory external standard calibrations of C_1-C_5 alkanoic acids using a dilution flow of humidified UZA effectively reproduce the RH matrix effects observed during standard addition calibrations performed at HOMEChem (described in section S4), further displaying the efficacy of this approach. Trends in I^- TOF-CIMS C_1-C_3 alkanoic acid sensitivities as a function of RH are consistent with previous work.[17]

We assess the RH-dependent sensitivity of N_2O_5 and $ClNO_2$ further by performing external standard calibrations under various humidity conditions. We observe a similar trend in humidity-dependent N_2O_5 I^- TOF-CIMS sensitivity to that observed by Kercher et al.[18] As humidity in the IMR increases, $IN_2O_5^-$ sensitivity increases and NO_3^- sensitivity decreases, while the total N_2O_5 sensitivity remains fairly constant (albeit decreases slightly with increasing humidity); indicating that the mass-dependent transmission efficiency of these compounds through the instrument is also fairly constant (Figure S12). $ClNO_2$ sensitivity does not vary significantly under the HOMEChem conditions as $P_{H2O,IMR} >$ 0.6 mbar (~30% RH measured in-line during HOMEChem) (Figure S13). This trend in RH-dependent I^- TOF-CIMS $ClNO_2$ sensitivity agrees with that observed by Kercher et al.[18]

We did not further assess RH-dependent I^- TOF-CIMS sensitivity for Cl_2 because the RH-dependent Cl_2 sensitivities reported by Lee et al.[17] were relatively invariable as $P_{H2O,IMR} > 0.4$ mbar. We anticipate a similar result as trends in RH-dependent I^- TOF-CIMS sensitivity are fairly consistent across instruments (irrespective of the absolute magnitude of these trends). We do not further characterize the RH-dependent I^- TOF-CIMS sensitivity of HOCl. Some variability in calculated HOCl mixing ratios may thus be caused by variations in ambient RH during HOMEChem. However, indoor RH typically varied ±2% during the experiments, and we expect a subsequently negligible fluctuation in I^- TOF-CIMS sensitivity to HOCl.

Our instrumental background measurements at HOMEChem were performed with dry (RH = 0%) UZA, and therefore may not be a true representation of analyte background signals measured in sampled indoor air (RH ≈ 55%, corresponding to $P_{H2O,IMR} \approx 1.4$ mbar in Austin, TX). To address this, we performed post-campaign measurements of I^- TOF-CIMS background signals for HOCl, Cl_2, Cl_2O, $ClNO_2$, $NHCl_2$, and NCl_3 (detected as $[I+M]^-$ adducts) while sampling UZA of variable RH. The RH of UZA (RH_{UZA}) during these experiments ranged from 0 – 70% (corresponding to $P_{H2O,IMR} = 0 – 1.4$ mbar in Fort Collins, CO). Instrumental background signals for all compounds tested were higher by a factor of 3 – 8 when $RH_{UZA} = 70\%$ compared to $RH_{UZA} = 0\%$. However, measured background signals for these compounds at HOMEChem were typically on the order of $10^0 – 10^1$ Hz, while respective measured signals reached orders of $10^4 – 10^5$ Hz during bleach cleaning. We therefore conclude that the lack of humidity in the I^- TOF-CIMS background measurements of these compounds performed during HOMEChem does not significantly impact their respective background-subtracted I^- TOF-CIMS signals (and subsequently mixing ratios) measured during bleach cleaning.

Section S6: Voltage scanning for I^- TOF-CIMS sensitivity estimation. Transmission of iodide-analyte adducts though the TOF-CIMS is controllable by systematically increasing (or 'scanning') the voltage gradient (dV), and therefore electric field strength, between any adjacent pair of ion optics components in the ion transmission region of the instrument.[8, 19] Increasing electric field strength leads to enhanced collisionally-induced dissociation of these adducts, and a decrease in their overall transmission. Cluster transmission decreases in a sigmoidal fashion with increasing dV.[8, 19] An important empirical parameter related to I^- TOF-CIMS sensitivity, dV_{50}, is calculated as the half-maximum of a sigmoidal fit to these data.[8, 19] dV_{50} is a proxy for I^- adduct binding enthalpy;[8] the strength of these adducts dictate their transmission through the instrument, thereby directly influencing TOF-CIMS sensitivity to these adducts.[8, 20]

In this study, we scanned the 'SSQ back - lens skimmer' component relation. Details of this component relation, and how we perform these voltage scanning experiments are found in Brophy and Farmer[19]. We plot the logarithm of I^- TOF-CIMS sensitivities for a variety of calibrant compounds (C_1-C_5 alkanoic acids, HNO_3, N_2O_5) against their respective dV_{50} values (Figure S14). We determined calibrant sensitivities via in-laboratory external standard calibrations performed shortly after HOMEChem (detailed in section S5). We also performed voltage scanning experiments during these calibration periods to determine calibrant dV_{50} values. We performed these experiments under variable $P_{H2O,IMR}$

settings (see section S5) to assess how ambient humidity affects the dV_{50}-sensitivity relationship (Figure S14). Here, we observe a linear (r^2 = 0.92-0.98) relationship between log(sensitivity) and dV_{50}, with linearity typically increasing as humidity increases. Further, the spread between linear fits in log(sensitivity) space decreases above 0.6 mbar, suggesting that variability in estimated sensitivity attributable to $P_{H2O,IMR}$ decreases with increasing water vapor present. Additionally, we performed voltage scanning during various periods throughout HOMEChem to determine dV_{50} values of gas-phase compounds present in ambient air (i.e during bleach cleaning).

We used this relationship as a model for sensitivity (and therefore mixing ratio) estimation by inputting dV_{50} values of compounds detected in ambient air during HOMEChem into the linear regressions used in Figure S14. We choose the dV_{50}-sensitivity relationship at $P_{H2O,IMR}$ = 1.5 mbar to estimate Cl_2O, $NHCl_2$, and NCl_3 sensitivities during HOMEChem, as these humidity settings most closely match those observed during bleach cleaning activities. We considered N_2O_5 a 'maximally' sensitive compound, in that it forms strongly bound adducts with I^- at the collision limit (see section S5).[8, 21] Therefore, any compound with a dV_{50} ≥ that of total N_2O_5 ($IN_2O_5^-$ + NO_3^-) (dV_{50} = 29.5 ± 0.5 V) was assigned the same sensitivity as total N_2O_5 (i.e. the 'collision-limit' sensitivity). Cl_2O and NCl_3 had higher dV_{50} values than N_2O_5 during HOMEChem (36. ± 2. V and 37.1 ± 0.3 V, respectively), and were therefore assigned the collision-limit sensitivity. $NHCl_2$ had a dV_{50} of 25.9 ± 0.8 V, and was assigned an estimated sensitivity of 10 ± 10 Hz $pptv^{-1}$. The large magnitude of error in estimated $NHCl_2$ sensitivity is associated with uncertainty in the dV_{50}-sensitivity relationship model.

The calibrant compounds used in the generation of this sensitivity estimation model are representative of those whose I^- adducts do not undergo substantial dissociation or fragmentation upon transmission through the TOF-CIMS. We note the abundance of ICl^- in our I^- TOF-CIMS spectra during bleach cleaning events at HOMEChem—likely a fragmentation product of labile chlorine-containing molecules initially bound to I^-. This observation is consistent with Wong et al.[22], who observed similar fragmentation in their I^- TOF-CIMS spectra during their indoor bleach cleaning measurements. We hypothesize that I^- adducts of many chlorine-containing molecules undergo fragmentation during their transmission through the TOF-CIMS, resulting in overestimated sensitivities (and therefore underestimated mixing ratios) from this model. Our model overestimates HOCl and $ClNO_2$ sensitivities by 1 and 3 orders of magnitude, respectively, which could be driven by adduct fragmentation. Reported Cl_2O, $NHCl_2$ and NCl_3 mixing ratios could therefore also be further underestimated from this fragmentation.

Supporting Figures

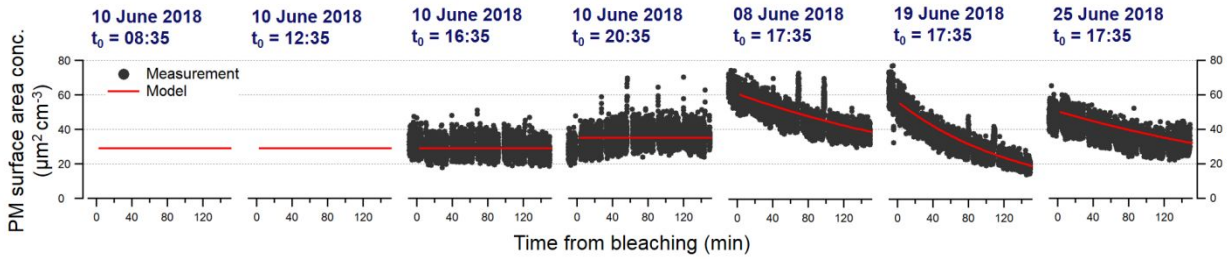

Figure S1. Measured indoor particulate matter (PM) surface area concentrations during various bleach cleaning experiments performed at HOMEChem (black markers). Red traces represent corresponding kinetic modeling results. t_0 indicates local times at which bleach mopping experiments began.

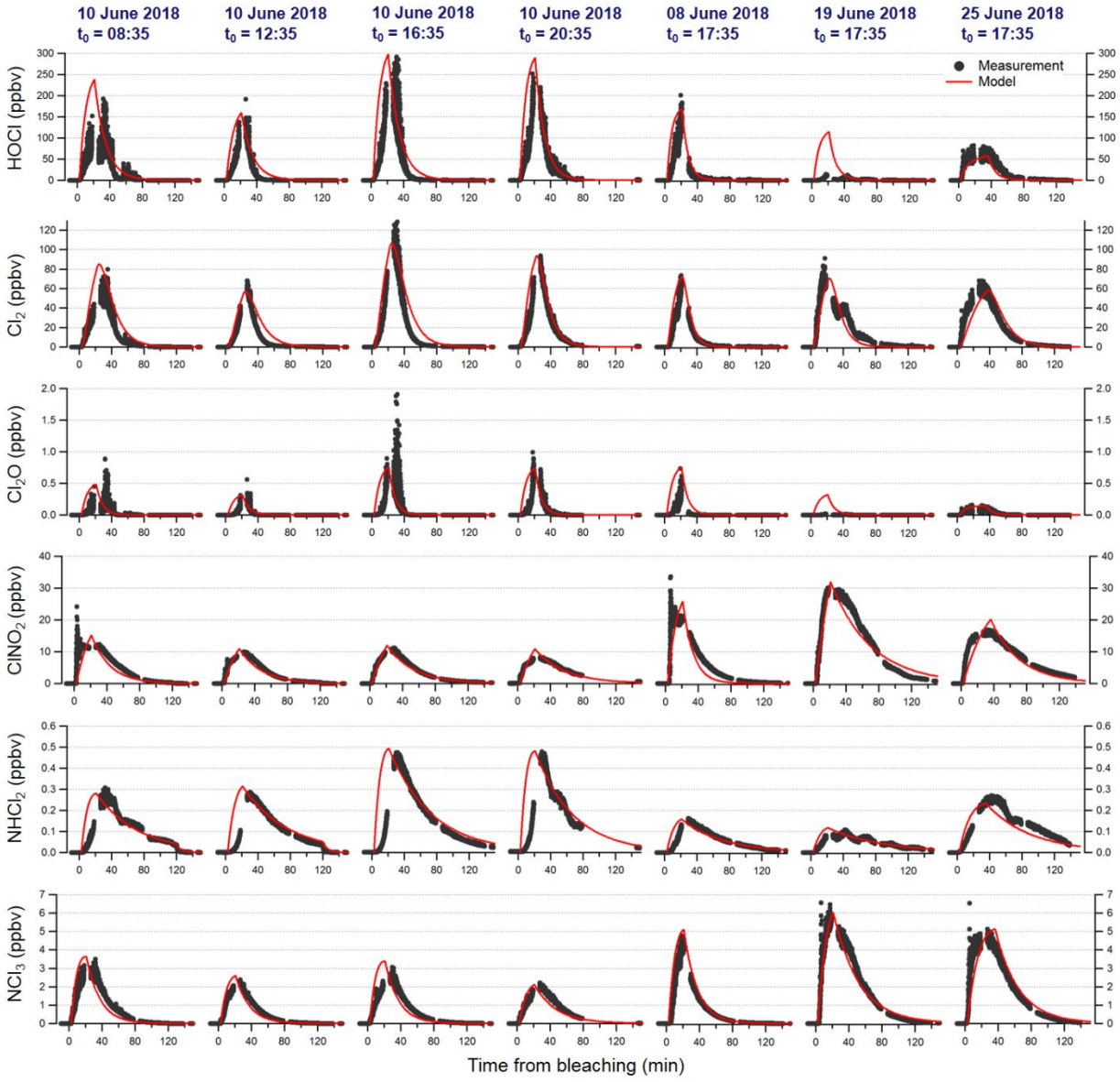

Figure S2. Measured indoor mixing ratios for HOCl, Cl_2, Cl_2O, $ClNO_2$, $NHCl_2$, and NCl_3 during various bleach cleaning experiments performed at HOMEChem (black markers). Red traces represent corresponding kinetic modeling results. t_0 indicates local times at which bleach mopping experiments began.

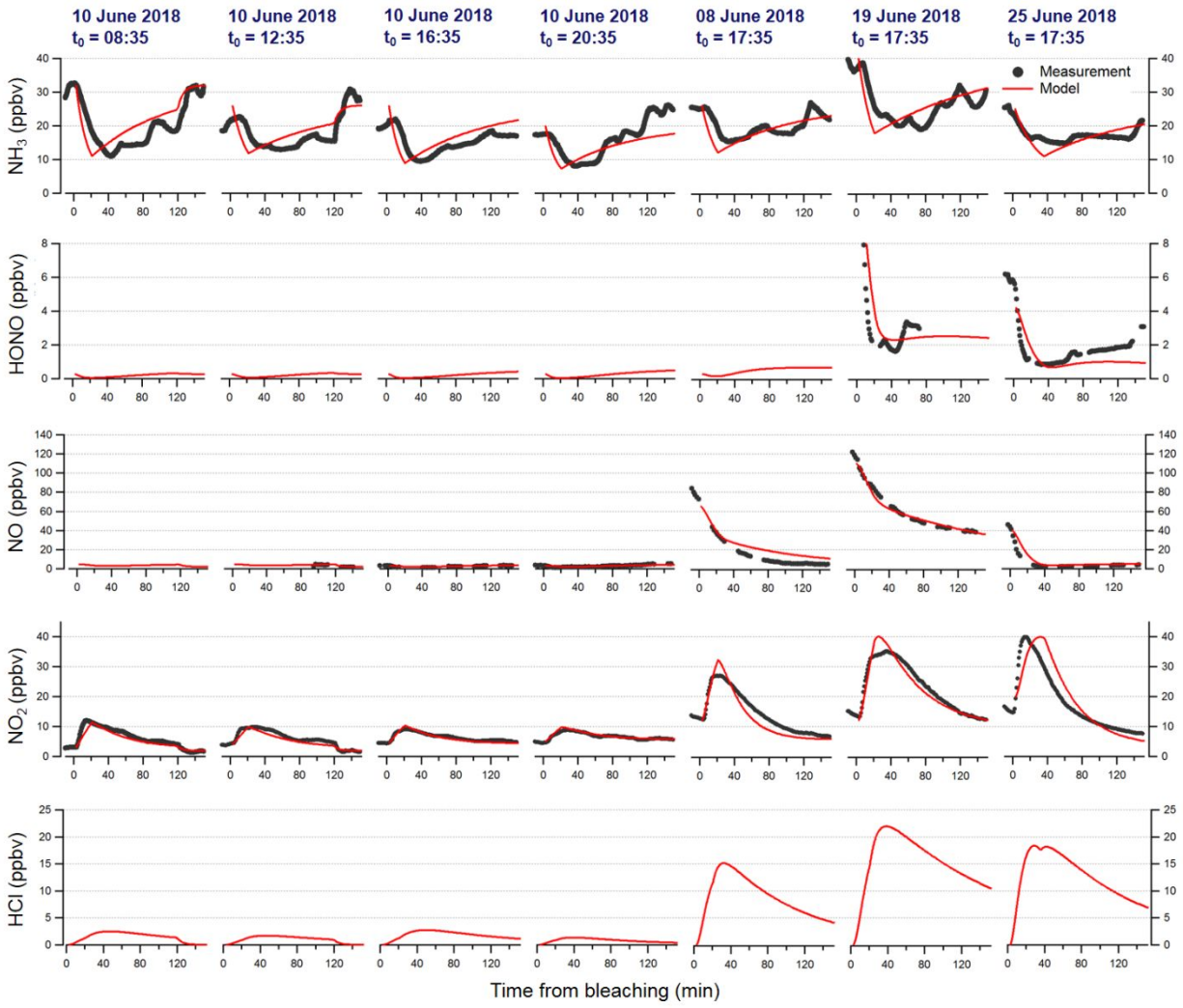

Figure S3. Measured indoor mixing ratios for NH_3, HONO, NO, and NO_2 during various bleach cleaning experiments performed at HOMEChem (black markers). Red traces represent kinetic modeling results for measured species, as well as predicted HCl mixing ratios. t_0 indicates local times at which bleach mopping experiments began.

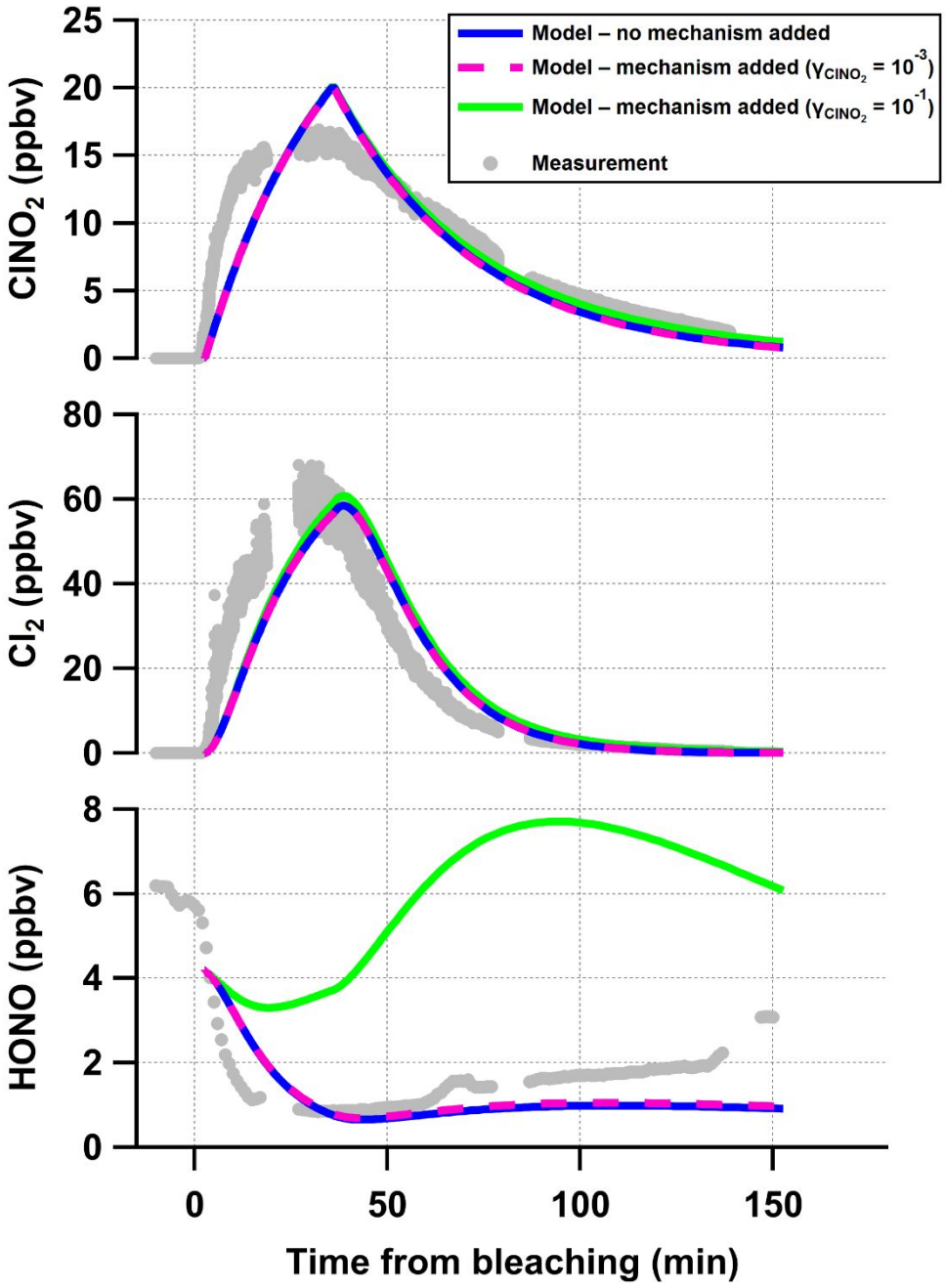

Figure S4. Kinetic model sensitivity test comparing indoor $ClNO_2$, Cl_2, and HONO mixing ratios during the inclusion of a heterogeneous $ClNO_2$ loss mechanism ($ClNO_2 + H^+ + Cl^- \rightarrow Cl_2 + HONO$) during a bleach cleaning experiment on 25 June 2018 at HOMEChem. Solid blue trace represents model results excluding this mechanism. Dashed pink and solid green traces represents model results including this mechanism using uptake coefficients (γ_{ClNO2}) of 10^{-3} and 10^{-1}, respectively. Grey markers represent HOMEChem measurement data. Bleach cleaning was performed at 17:35 local time, and lasted approximately 10 minutes.

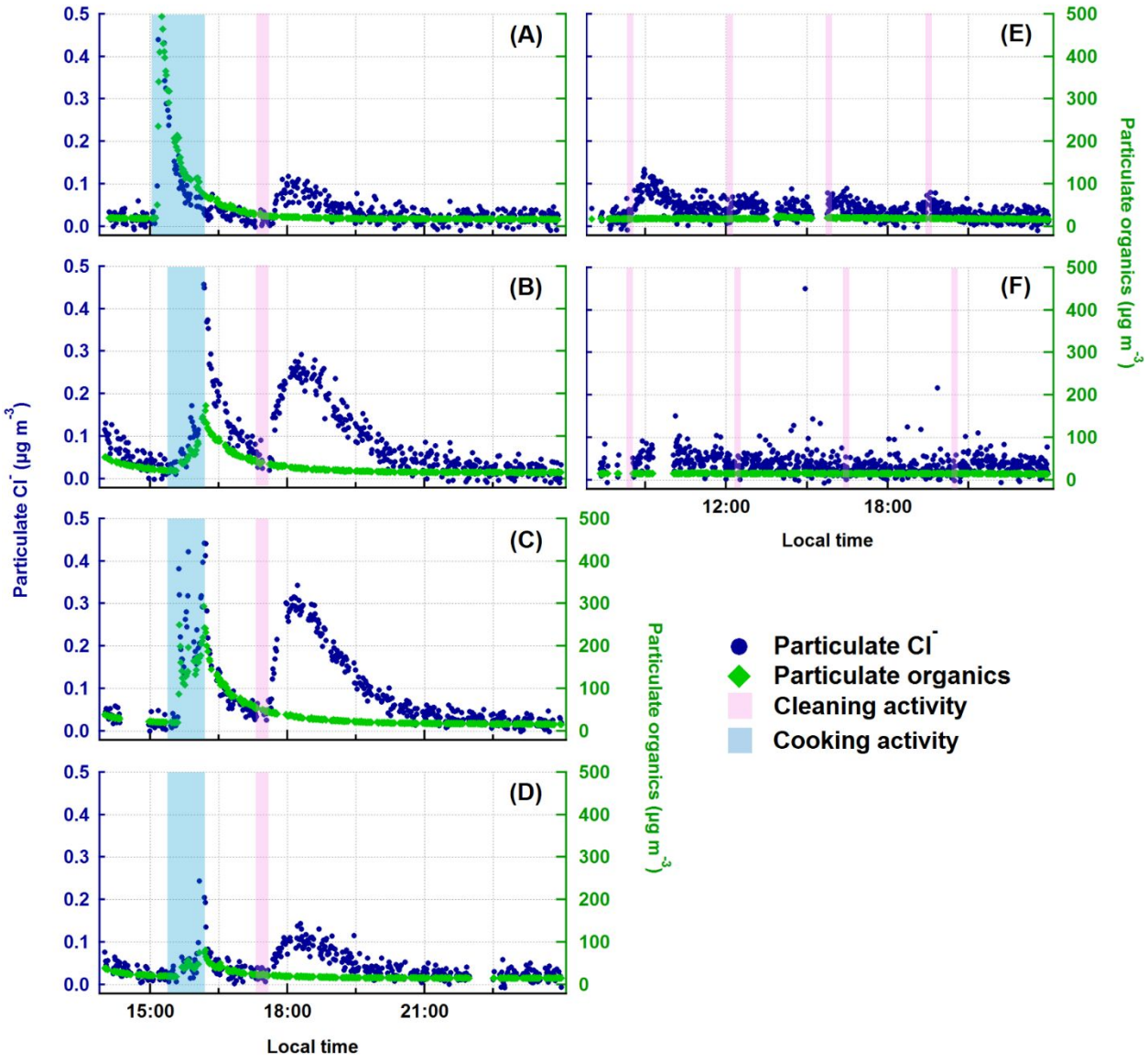

Figure S5. Indoor particulate Cl^- (blue markers) and organic (green markers) mass concentrations during layered experiments on (A) 08, (B) 19, (C) 21, and (D) 25 June 2018; and sequential experiments on (E) 07 and (F) 10 June 2018. Shaded pink and blue regions correspond to local time during which bleach cleaning and cooking events took place, respectively. We use particulate organic mass concentration here as a proxy for total indoor PM mass concentration.

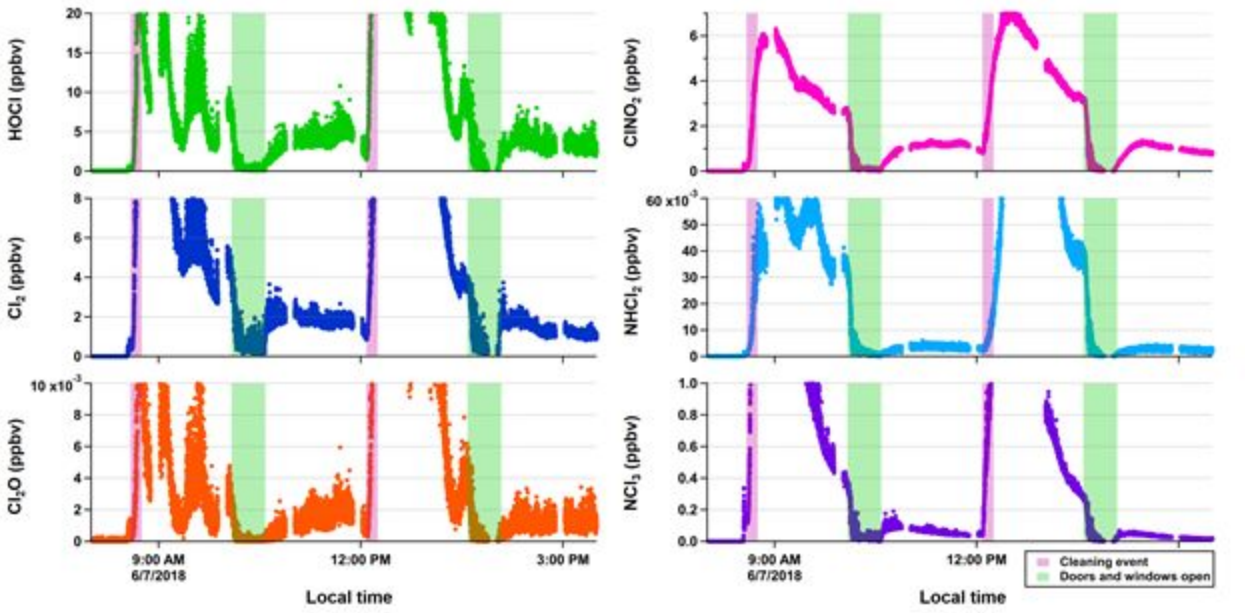

Figure S6. Indoor mixing ratio time series data (colored markers) for HOCl, Cl_2, Cl_2O, $ClNO_2$, $NHCl_2$, and NCl_3 during a bleach cleaning experiment on 07 June 2018. Shaded pink and green regions correspond to local time during which bleach cleaning and door/window opening took place, respectively.

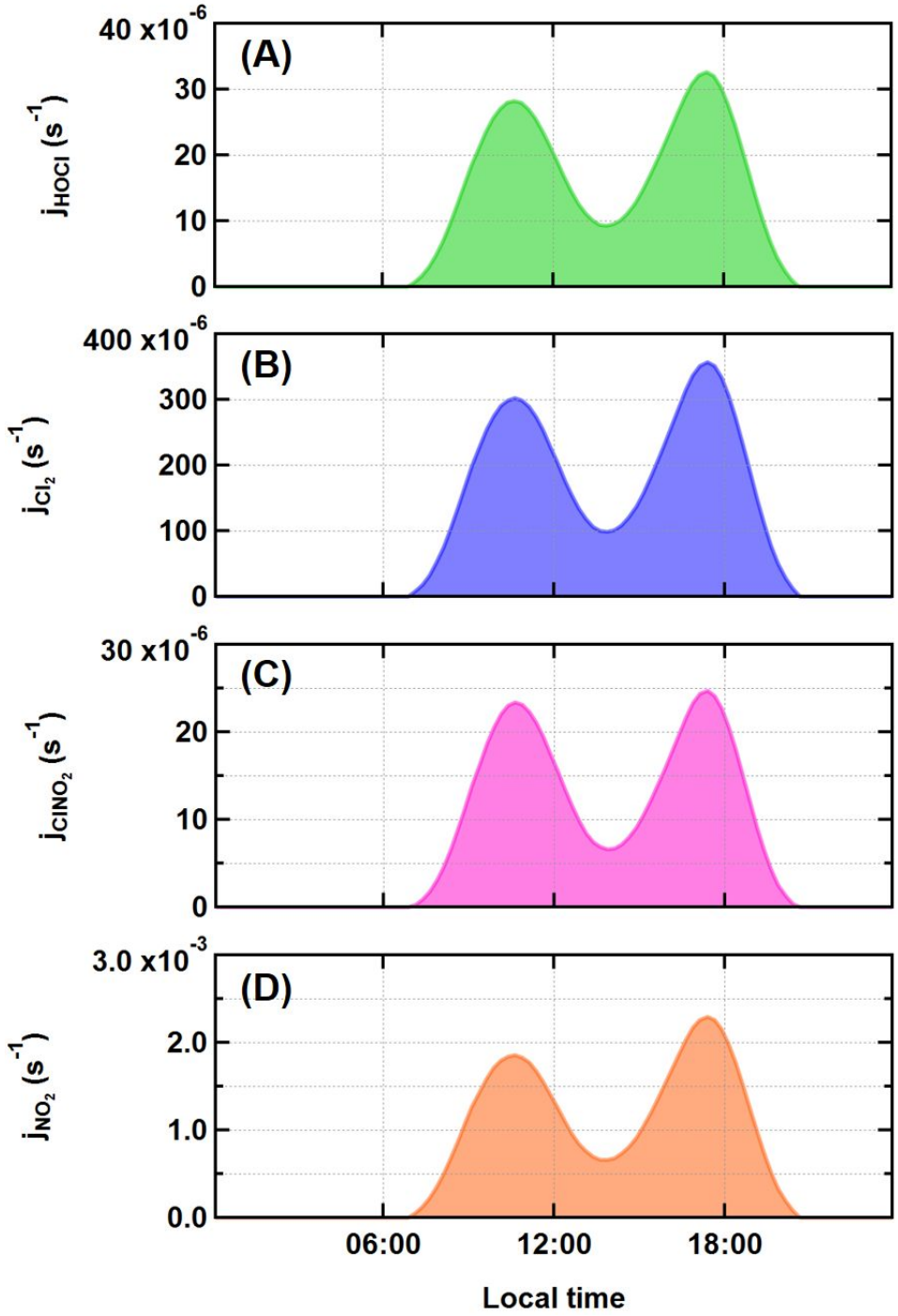

Figure S7. Upper-bound diel profiles of indoor photolysis rates for (A) HOCl, (B) Cl_2, (C) $ClNO_2$, and (D) NO_2 for the duration of HOMEChem.

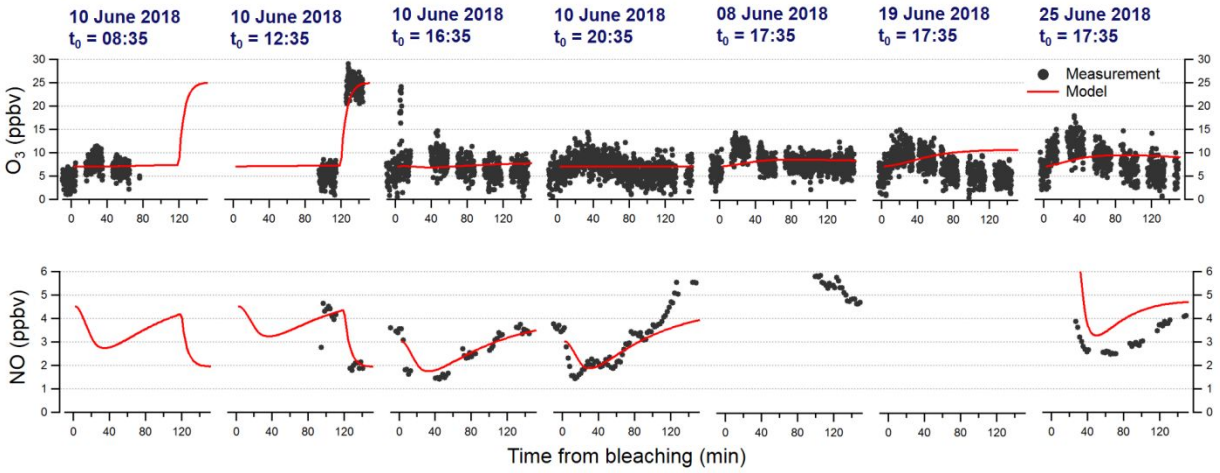

Figure S8. Measured indoor mixing ratios for O_3 and NO during various bleach cleaning experiments performed at HOMEChem (black markers). Red traces represent corresponding kinetic modeling results. t_0 indicates local times at which bleach mopping experiments began. Note the different scale used for NO here compared to Figure S3.

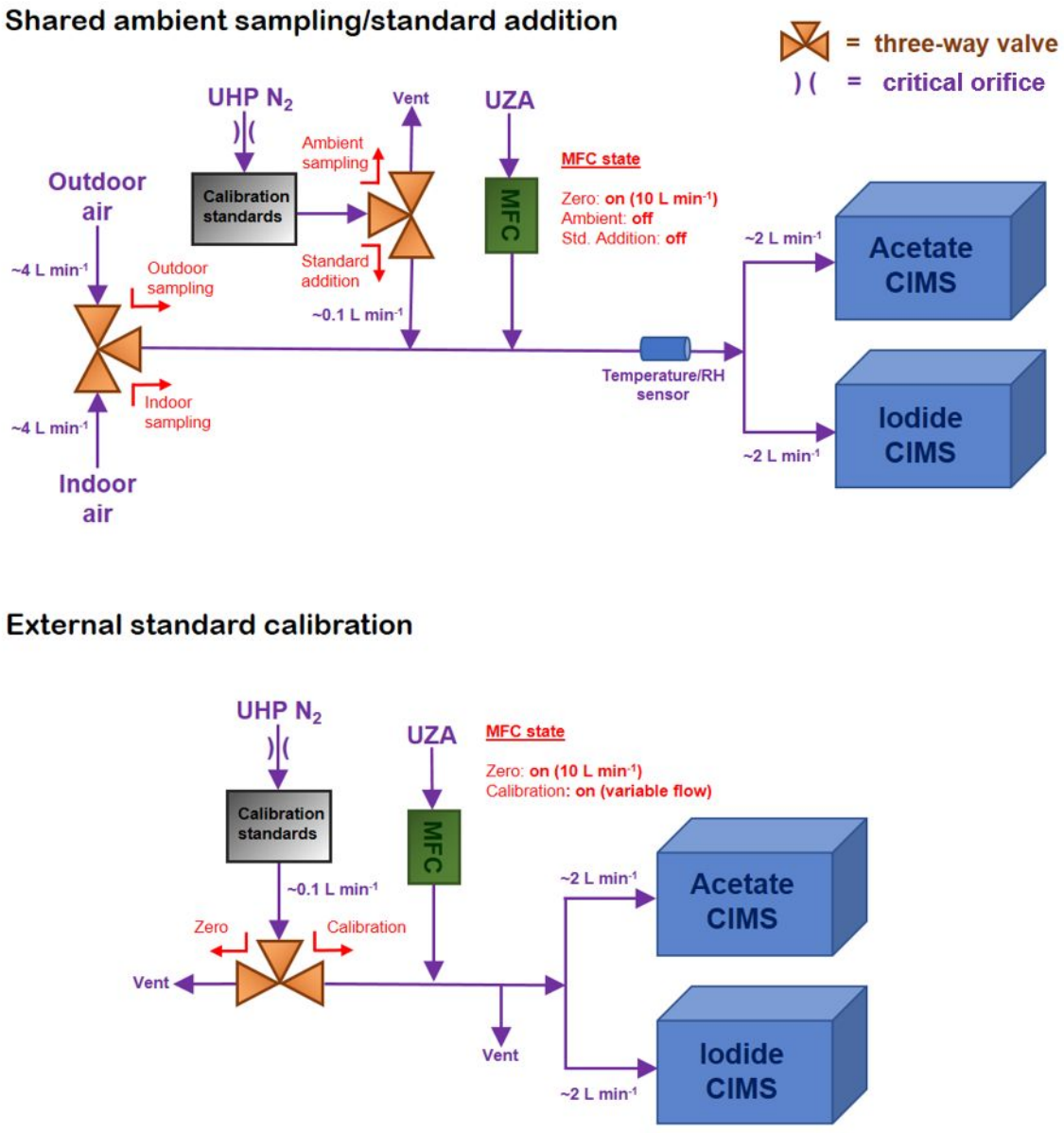

Figure S9. Schematic of shared inlet and calibration system used during HOMEChem during ambient sampling/standard addition (top), and external standard calibration regimes (bottom). Red arrows indicate direction of three-way valves during different sampling/calibration regimes. MFC = mass-flow controller.

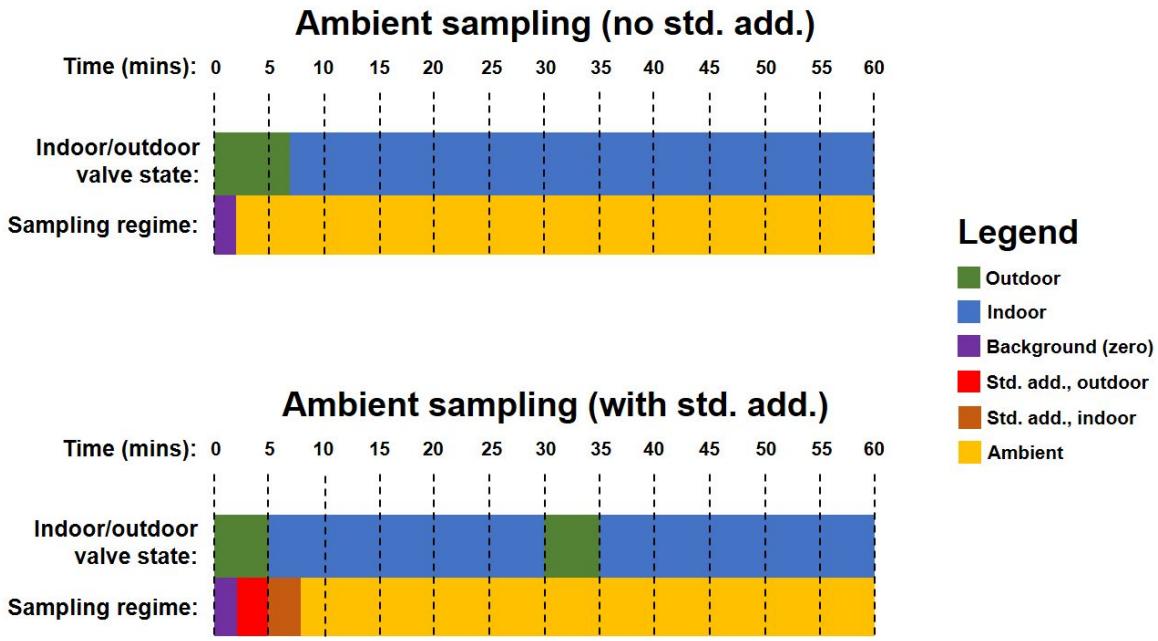

Figure S10. Timing scheme for instrumental backgrounds and indoor/outdoor ambient sampling without (top) and with (bottom) standard additions (abbreviated here as "std. add.") included.

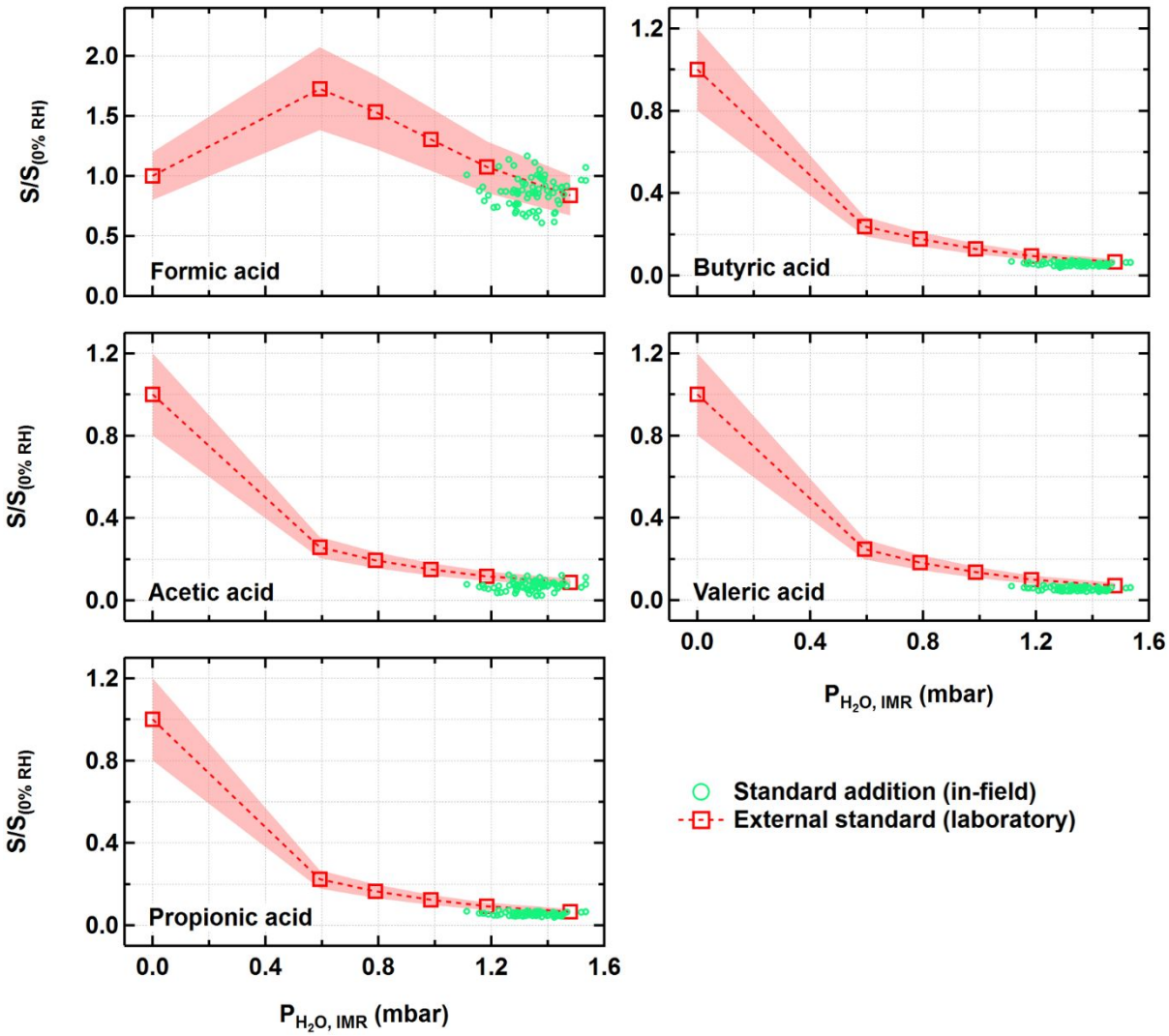

Figure S11. Standard addition I^- TOF-CIMS sensitivities from HOMEChem (green dots), and RH-dependent external standard I^- CIMS sensitivities (red markers) for C_1-C_5 alkanoic acids, plotted as a function of water vapor partial pressure in the IMR ($P_{H2O,IMR}$). Red markers and shaded regions represent means and uncertainties of triplicate external standard calibration sensitivity measurements. Here, sensitivities (S) are reported relative to CIMS sensitivity at 0% RH ($S_{(0\%\ RH)}$).

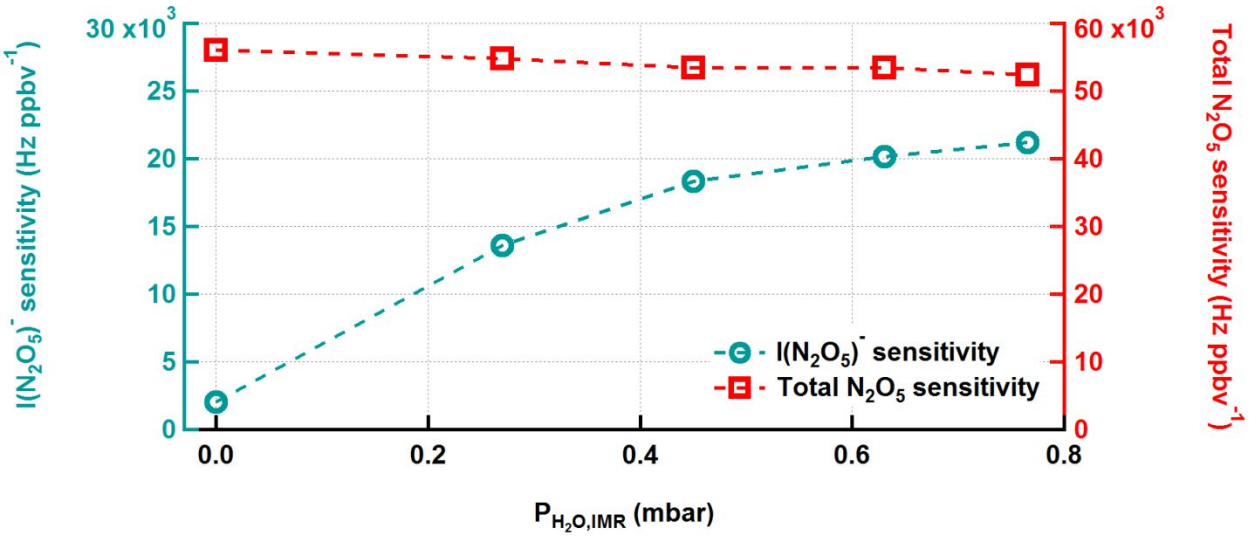

Figure S12. I^- TOF-CIMS sensitivities for $IN_2O_5^-$ (teal circles, left vertical axis) and total N_2O_5 (red squares, right vertical axis) measured as a function of water vapor partial pressure in the IMR ($P_{H2O,IMR}$). Markers represent means of each calibration. We exclude error bars for clarity. Here, 'total N_2O_5' corresponds to $IN_2O_5^-$ + NO_3^-.

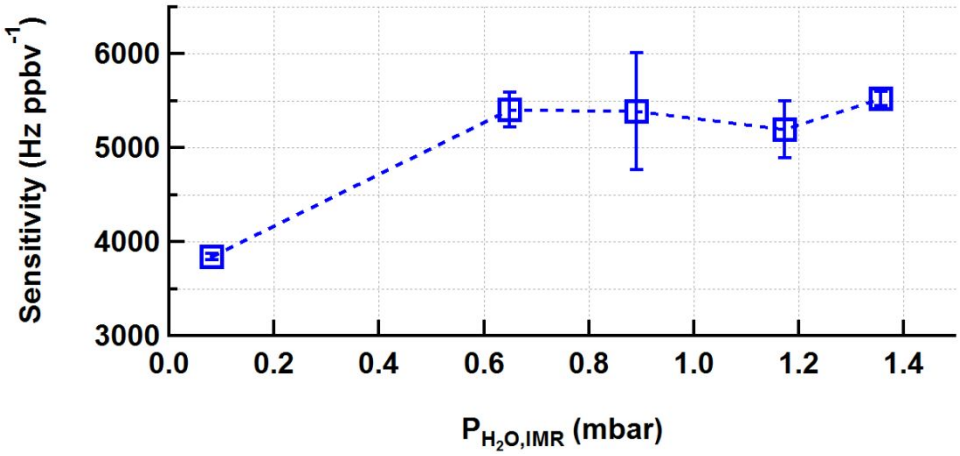

Figure S13. $ClNO_2$ I^- TOF-CIMS sensitivities measured as a function of water vapor partial pressure in the IMR ($P_{H2O,IMR}$). Markers and error bars represent means and uncertainties of each calibration.

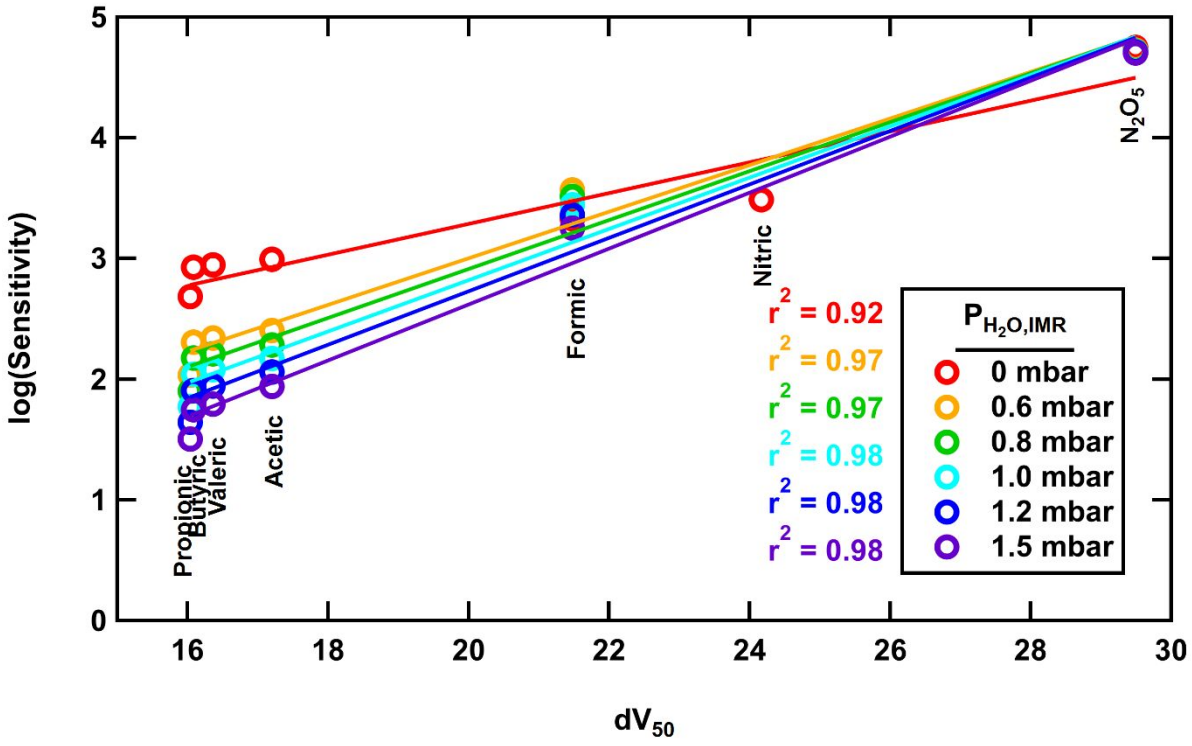

Figure S14. Relationship between the logarithm of I^- TOF-CIMS sensitivity and dV_{50} for several calibrant compounds (colored markers). Solid colored traces represent linear fits to the data using a least orthogonal distance regression (ODR) fitting method. Markers, linear fits, and r^2 values are colored by $P_{H2O,IMR}$ values (see figure legend). N_2O_5 sensitivity corresponds to 'total N_2O_5' ($IN_2O_5^-$ + NO_3^-). We are only able to report HNO_3 sensitivity at $P_{H2O,IMR}$ = 0 mbar. Vertical text labels correspond to approximate locations of calibrant compounds in dV_{50} space.

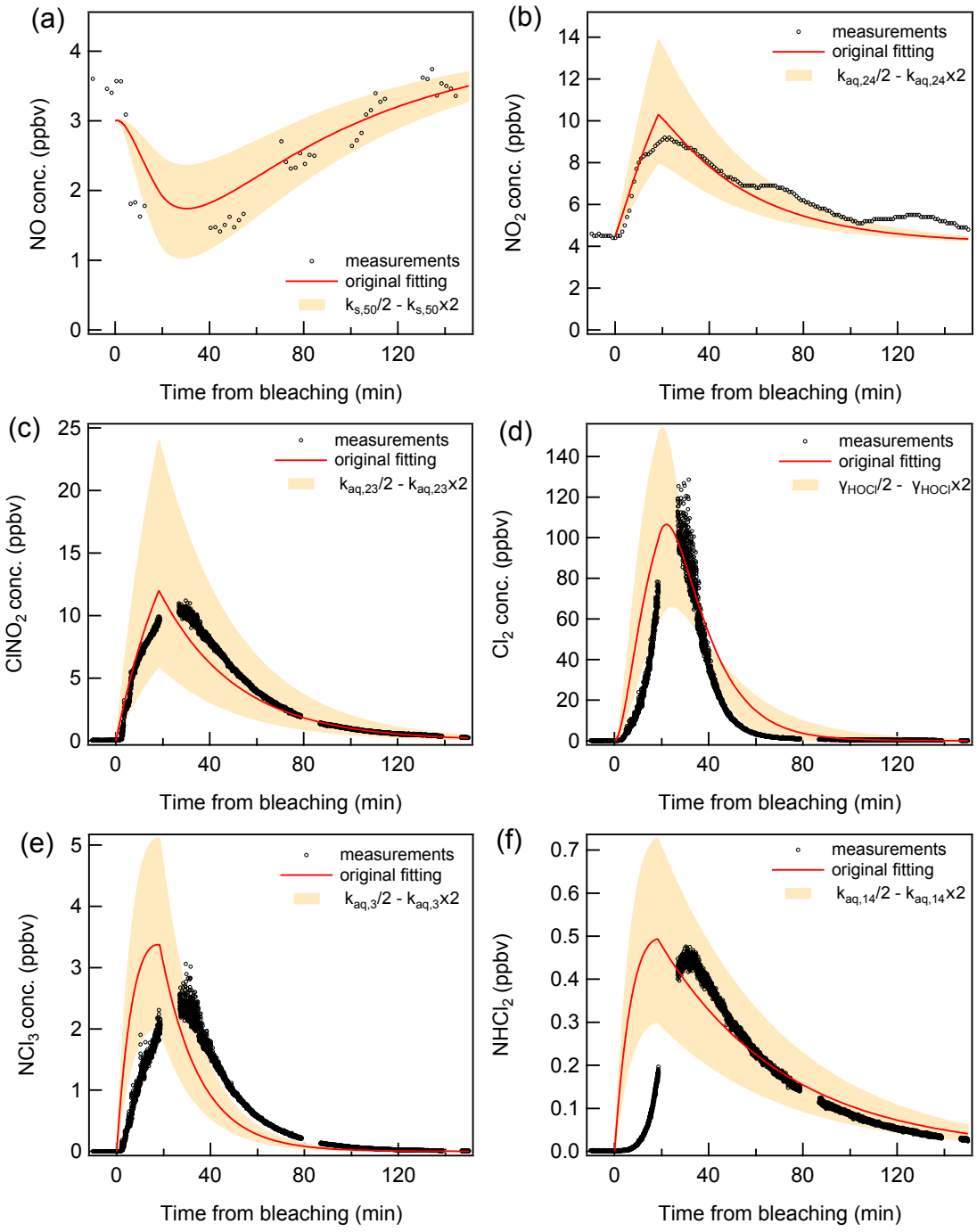

Figure S15. Sensitivity tests showing the impact of increasing or decreasing selected parameters on model outputs of gas-phase concentrations of selected chemical species. Parameters were typically varied by a factor of two. The target parameter and chosen range is shown in each sub-figure legend. For example, panel (d) shows the impact on Cl_2 concentration from varying the uptake coefficient of HOCl by a factor of 2 (shaded yellow region) from the base case scenario (red line, corresponds to values summarized in Table S4).

Supporting Tables

Table S1 – Aqueous chemical mechanisms in the applied bleach used in kinetic model.

Reaction number	Reaction	Rate	Reference or comment
1	$NH_3 + HOCl \rightarrow NH_2Cl + H_2O$	$k_{aq,1} = 6.9 \times 10^{-15}\ cm^3\ s^{-1}$	Jafvert and Valentine[23]
2	$NH_2Cl + HOCl \rightarrow NHCl_2 + H_2O$	$k_{aq,2} = 4.6 \times 10^{-17}\ cm^3\ s^{-1}$ *	Jafvert and Valentine[23]
3	$NHCl_2 + HOCl \rightarrow NCl_3 + H_2O$	$k_{aq,3}$ = see Table S4 **	Jafvert and Valentine[23]
4	$NH_2Cl + H_2O \rightarrow HOCl + NH_3$	$k_{aq,4} = 2.1 \times 10^{-5}\ s^{-1}$	Jafvert and Valentine[23]
5	$NHCl_2 + H_2O \rightarrow HOCl + NH_2Cl$	$k_{aq,5} = 6.4 \times 10^{-7}\ s^{-1}$	Jafvert and Valentine[23]
6	$NH_2Cl + NH_2Cl + H^+ \rightarrow NHCl_2 + NH_3$	$k_{aq,6} = 1.9 \times 10^{-38}\ cm^6\ s^{-1}$	Jafvert and Valentine[23]
7	$NHCl_2 + NH_3 + H^+ \rightarrow NH_2Cl + NH_2Cl$	$k_{aq,7} = 1.7 \times 10^{-37}\ cm^6\ s^{-1}$	Jafvert and Valentine[23]
8	$NHCl_2 + OH^- \rightarrow I$	$k_{aq,8} = 1.9 \times 10^{-19}\ cm^3\ s^{-1}$	Jafvert and Valentine[23]
9	$I + NHCl_2 \rightarrow HOCl + Products$	$k_{aq,9} = 4.6 \times 10^{-17}\ cm^3\ s^{-1}$	Jafvert and Valentine[23]
10	$I + NH_2Cl \rightarrow Products$	$k_{aq,10} = 1.4 \times 10^{-17}\ cm^3\ s^{-1}$	Jafvert and Valentine[23]
11	$NH_2Cl + NHCl_2 \rightarrow Products$	$k_{aq,11} = 2.5 \times 10^{-23}\ cm^3\ s^{-1}$	Jafvert and Valentine[23]
12	$NHCl_2 + NCl_3 + OH^- \rightarrow 2\ HOCl + Products$	$k_{aq,12} = 1.5 \times 10^{-31}\ cm^6\ s^{-1}$	Jafvert and Valentine[23]
13	$NH_2Cl + NCl_3 + OH^- \rightarrow HOCl + Products$	$k_{aq,13} = 3.8 \times 10^{-33}\ cm^6\ s^{-1}$	Jafvert and Valentine[23]
14***	$NHCl_2 + 2HOCl + H_2O \rightarrow HNO_3 + 4HCl$	$k_{aq,14}$ = see Table S4	Jafvert and Valentine[23]
15	$OCl^- + H^+ \rightarrow HOCl$	$k_{aq,15} = 1.0 \times 10^{-11}\ cm^3\ s^{-1}$	assumed to be fast
16	$HOCl \rightarrow H^+ + OCl^-$	$k_{aq,16} = k_{aq,15} \times (6.02 \times 10^{23}/1000) \times 2.9 \times 10^{-8}\ s^{-1}$	based on a K_a value of 2.9×10^{-8}; Deborde and Von Gunten[24]
17	$HOCl + H^+ + Cl^- \rightarrow Cl_2 + H_2O$	$k_{aq,17} = 1.2 \times 10^{-37}\ cm^6\ s^{-1}$	Deborde and Von Gunten[24]
18	$H_2O + Cl_2 \rightarrow HOCl + H^+ + Cl^-$	$k_{aq,18} = 22.3\ s^{-1}$	Deborde and Von Gunten[24]
19	$H^+ + Cl^- \rightarrow HCl$	$k_{aq,19} = 1.0 \times 10^{-11}\ cm^3\ s^{-1}$	assumed to be fast
20	$HCl \rightarrow H^+ + Cl^-$	$k_{aq,20} = k_{aq,19} \times (6.02 \times 10^{23}/1000) \times 1.3 \times 10^{6}\ s^{-1}$	based on a K_a value of 1.3×10^{6}

21	$HOCl + HOCl \rightarrow Cl_2O + H_2O$	$k_{aq,21} = 3.0 \times 10^{-23}$ cm^3 s^{-1}	fitting parameter
22	$Cl_2O + H_2O \rightarrow HOCl + HOCl$	$k_{aq,22} = k_{aq,21} \times (6.02 \times 10^{23}/1000) \times 8.7 \times 10^{-3}$ s^{-1}	based on a K_a value of 8.7×10^{-3}; Deborde and Von Gunten[24]
23	$HOCl + (NO_2^-) \rightarrow ClNO_2 + OH^-$	$k_{aq,23}$ = see Table S4	Eiserich et al.[25]
24	$ClNO_2 + (NO_2^-) \rightarrow 2\ NO_2 + Cl^-$	$k_{aq,24}$ = see Table S4	Frenzel et al.[26]

* Increased from a literature value of 4.6×10^{-19} cm^3 s^{-1} in order to fit the data and in order to not be significantly lower than $k_{aq,3}$. This may be due to specific experimental conditions affecting bleach solution pH and/or composition.

** The literature value was $4.6 \times 10^{-37}[OCl^-] + 9.0 \times 10^{-33}[OH^-]$ cm^3 s^{-1} but was simplified and varied until the data could be fitted as shown in Table S4.

*** The rate expression is $k_{aq,14}[NHCl_2][OCl^-]$. $k_{aq,14}$ was varied around the literature value of 3.8×10^{-19} cm^3 s^{-1} until the data could be fitted and values are close to the original value.

Table S2 – Gas-phase and heterogeneous chemistry used in kinetic model.

Reaction number	Reaction	Rate	Reference or comment
1	$Cl_2 + h\nu \rightarrow 2Cl$	j_{Cl2} = see Table S4	Xue et al.[3]
2	$HOCl + h\nu \rightarrow OH + Cl$	j_{HOCl} = see Table S4	Xue et al.[3]
3	$ClNO_2 + h\nu \rightarrow NO_2 + Cl$	j_{ClNO2} = see Table S4	Xue et al.[3]
4	$ClONO_2 + h\nu \rightarrow NO_3 + Cl$	$k_{g,4} = 0.83 \times j_{ClNO2}$	Xue et al.[3]
5	$ClONO_2 + h\nu \rightarrow NO_2 + ClO$	$k_{g,5} = 0.17 \times j_{ClNO2}$	Xue et al.[3]
6	$NO_2 + NO_3 \rightarrow N_2O_5$	$k_{g,6} = 1.9 \times 10^{-12}$ cm^3 s^{-1}	Atkinson et al.[27]
7	$N_2O_5 \rightarrow NO_2 + NO_3$	$k_{g,7} = 6.9 \times 10^{-2}$ s^{-1}	Atkinson et al.[27]
8	$Cl + O_3 \rightarrow ClO + O_2$	$k_{g,8} = 2.8 \times 10^{-11} \times \exp(-250/T)$ cm^3 s^{-1}	Xue et al.[3]
9	$Cl + HO_2 \rightarrow HCl + O_2$	$k_{g,9} = 3.5 \times 10^{-11}$ cm^3 s^{-1}	Xue et al.[3]
10	$Cl + HO_2 \rightarrow ClO + OH$	$k_{g,10} = 7.5 \times 10^{-11} \times \exp(-620/T)$ cm^3 s^{-1}	Xue et al.[3]
11	$Cl + H_2O_2 \rightarrow HCl + HO_2$	$k_{g,11} = 1.1 \times 10^{-11} \times \exp(-980/T)$ cm^3 s^{-1}	Xue et al.[3]
12	$Cl + NO_3 \rightarrow NO_2 + ClO$	$k_{g,12} = 2.4 \times 10^{-11}$ cm^3 s^{-1}	Xue et al.[3]
13	$Cl + ClONO_2 \rightarrow Cl_2 + NO_3$	$k_{g,13} = 6.2 \times 10^{-12} \times \exp(-145/T)$ cm^3 s^{-1}	Xue et al.[3]
14	$OH + HCl \rightarrow Cl + H_2O$	$k_{g,14} = 1.7 \times 10^{-12} \times \exp(-230/T)$ cm^3 s^{-1}	Xue et al.[3]

15	$OH + Cl_2 \rightarrow HOCl + Cl$	$k_{g,15} = 3.6 \times 10^{-12} \times \exp(-1200/T)$ $cm^3\ s^{-1}$	Xue et al.[3]
16	$OH + HOCl \rightarrow ClO + H_2O$	$k_{g,16} = 5.0 \times 10^{-13}\ cm^3\ s^{-1}$	Xue et al.[3]
17	$OH + ClO \rightarrow HO_2 + Cl$	$k_{g,17} = 1.8 \times 10^{-11}\ cm^3\ s^{-1}$	Xue et al.[3]
18	$OH + ClO \rightarrow HCl + O_2$	$k_{g,18} = 1.2 \times 10^{-12}\ cm^3\ s^{-1}$	Xue et al.[3]
19	$ClO + NO_2 \rightarrow ClONO_2$	$k_{g,19} = 2.0 \times 10^{-11}\ cm^3\ s^{-1}$ *	Xue et al.[3]
20	$ClO + HO_2 \rightarrow HOCl + O_2$	$k_{g,20} = 2.2 \times 10^{-12} \times \exp(340/T)\ cm^3\ s^{-1}$	Xue et al.[3]
21	$ClO + NO \rightarrow Cl + NO_2$	$k_{g,21} = 6.2 \times 10^{-12} \times \exp(295/T)\ cm^3\ s^{-1}$	Xue et al.[3]
22**	$N_2O_5 + Aerosol \rightarrow Products$	$k_{g,22} = 0.25 \times \omega_{N2O5} \times \gamma_{N2O5} \times S_{AERO} \times (1 - \varphi_{ClNO2})\ s^{-1}$ ($\gamma_{N2O5} = 1 \times 10^{-2}$, φ_{ClNO2}=0.5)	Xue et al.[3]; Wong et al.[22]
23**	$N_2O_5 + Aerosol \rightarrow ClNO_2 + Products$	$k_{g,23} = 0.25 \times \omega_{N2O5} \times \gamma_{N2O5} \times S_{AERO} \times \varphi_{ClNO2}\ s^{-1}$ ($\gamma_{N2O5} = 1 \times 10^{-2}$, φ_{ClNO2}=0.5)	Xue et al.[3]; Wong et al.[22]
24**	$NO_3 + Aerosol \rightarrow Products$	$k_{g,24} = 0.25 \times \omega_{NO3} \times \gamma_{NO3} \times S_{AERO}\ s^{-1}$ ($\gamma_{NO3} = 4 \times 10^{-3}$)	Xue et al.[3]; Wong et al.[22]
25**	$ClONO_2 + Aerosol \rightarrow Cl_2 + HNO_3$	$k_{g,25} = 0.25 \times \omega_{ClONO2} \times \gamma_{ClONO2} \times S_{AERO}\ s^{-1}$ ($\gamma_{ClONO2} = 1 \times 10^{-2}$)	Xue et al.[3]; Wong et al.[22]
26**	$HOCl + Aerosol \rightarrow Cl_2$	$k_{g,26} = 0.25 \times \omega_{HOCl} \times \gamma_{HOCl} \times S_{AERO}\ s^{-1}$ ($\gamma_{HOCl} = 0.4$)	Xue et al.[3]; fitting parameter
27	$Cl + (VOCs) \rightarrow HCl + (VOCs)$	$k_{g,27} = 3\ s^{-1}$	assumed to be fast
28	$OH + (VOCs) \rightarrow (VOCs)$	$k_{g,28} = 3\ s^{-1}$	assumed to be fast
29	$N_2O_5 + HCl \rightarrow ClNO_2 + HNO_3$	$k_{g,29} = 6.7 \times 10^{-21}\ cm^3\ s^{-1}$	Wilkins Jr and Hisatsune[28]
30	$NO_2 + hv \rightarrow NO + O$	j_{NO2} = see Table S4	
31	$NO_3 + hv \rightarrow NO_2 + O$	j_{NO3} = see Table S4	
32	$HONO + hv \rightarrow NO + OH$	j_{HONO} = see Table S4	
33	$OH + O_3 \rightarrow HO_2 + O_2$	$k_{g,33} = 7.3 \times 10^{-14}\ cm^3\ s^{-1}$	Atkinson et al.[27]
34	$HO_2 + NO \rightarrow OH + NO_2$	$k_{g,34} = 8.8 \times 10^{-12}\ cm^3\ s^{-1}$	Atkinson et al.[27]
35	$HO_2 + O_3 \rightarrow OH + 2O_2$	$k_{g,35} = 2.0 \times 10^{-15}\ cm^3\ s^{-1}$	Atkinson et al.[27]
36**	$NO_2 + Aerosol \rightarrow Product$	$k_{g,36} = 0.25 \times \omega_{NO2} \times \gamma_{NO2} \times S_{AERO}\ s^{-1}$ (γ_{NO2} = see Table S4)	fitting parameter
37**	$HO_2 + Aerosol \rightarrow Product$	$k_{g,37} = 0.25 \times \omega_{HO2} \times \gamma_{HO2} \times S_{AERO}\ s^{-1}$ ($\gamma_{HO2} = 0.5$)	George et al.[29]
38	$OH + NO \rightarrow HONO$	$k_{g,38} = 3.3 \times 10^{-11}\ cm^3\ s^{-1}$	Atkinson et al.[27]
39	$OH + HONO \rightarrow NO_2 + H_2O$	$k_{g,39} = 6.0 \times 10^{-12}\ cm^3\ s^{-1}$	Atkinson et al.[27]
40	$HOCl + NO \rightarrow NO_2 + HCl$	$k_{g,40} = 1.0 \times 10^{-18}\ cm^3\ s^{-1}$	Cook et al.[30]

41	$O + O_2 + M \rightarrow O_3 + M$	$k_{g,41} = 6.0 \times 10^{-34}\ cm^6\ s^{-1}$	Atkinson et al.[27]
42	$O + NO_2 + M \rightarrow NO_3 + M$	$k_{g,42} = 1.3 \times 10^{-31}\ cm^6\ s^{-1}$	Atkinson et al.[27]
43	$O + NO + M \rightarrow NO_2 + M$	$k_{g,43} = 1.0 \times 10^{-31}\ cm^6\ s^{-1}$	Atkinson et al.[27]
44***	$Cl_2 \rightarrow$ Products (on surfaces)	$k_{s,44}$ = see Table S4	fitting parameter
45***	$ClNO_2 \rightarrow$ Products (on surfaces)	$k_{s,45}$ = see Table S4	fitting parameter
46***	$NCl_3 \rightarrow$ Products (on surfaces)	$k_{s,46}$ = see Table S4	fitting parameter
47***	$Cl_2O \rightarrow$ Products (on surfaces)	$k_{s,47} = 2.0 \times 10^{-3}\ s^{-1}$	fitting parameter
48***	$NO_2 \rightarrow$ HONO (on surfaces)	$k_{s,48} = 1.4 \times 10^{-5}\ s^{-1}$	fitting parameter
49***	$NHCl_2 \rightarrow$ Products (on surfaces)	$k_{s,49} = 1.4 \times 10^{-4}\ s^{-1}$	fitting parameter
50***	$HOCl + NO \rightarrow NO_2 + HCl$ (on surfaces)	$k_{s,50}$ = see Table S4	fitting parameter
51***	$HOCl + HONO \rightarrow$ Products (on surfaces)	$k_{s,51}$ = see Table S4	fitting parameter

* The literature value was $7.0 \times 10^{-11}\ cm^3\ s^{-1}$ but was decreased slightly to fit the data.

** ω_X is the molecular speed of species X, γ_X is the uptake coefficient of species X, and S_{AERO} is the aerosol surface area concentration.

*** These reactions are assumed to occur on surfaces but are treated as losses from the gas-phase. They may also include currently unknown gas-phase reactions.

Table S3 – Henry's Law and gas-phase diffusion coefficients used in kinetic model.

Species	Henry's Law coefficient (mol $cm^{-3}\ atm^{-1}$)*	Gas-phase diffusion coefficient ($cm^2\ s^{-1}$)**
NH_3	0.06	0.23
NCl_3	9.9×10^{-5}	0.096
$NHCl_2$	2.9×10^{-2}	0.11
HOCl	0.6	0.15
Cl_2	9.2×10^{-5}	0.13
NH_2Cl	8.6×10^{-2}	0.14
HCl	0.72	0.17
I (intermediate)	Non-volatile	N/A
OCl-	Non-volatile	N/A
Cl	2.3×10^{-3}	0.18
OH	0.03	0.24****
$ClNO_2$	4×10^{-5}	0.12

NO_2	1.4×10^{-5}	0.17
$ClONO_2$	0.011 ***	0.11
NO_3	3.4×10^{-5}	0.15
ClO	7.0×10^{-4}	0.16
N_2O_5	2.1×10^{-3}	0.11
O_3	1×10^{-5}	0.18
HO_2	5	0.20
H_2O_2	70	0.19
NO	1.9×10^{-6}	0.20
HNO_3	210	0.14
Cl^-	Non-volatile	N/A
Cl_2O	1.7×10^{-2}	0.12
HONO	0.048	0.16
O	1×10^{-5} *****	0.32

* From Sander[31] unless otherwise stated.

** From https://www3.epa.gov/ceampubl/learn2model/part-two/onsite/estdiffusion-ext.html unless otherwise stated.
*** From Shi et al.[32].
**** From Tang et al.[33].
***** Assumed to be the same as O_3.

Table S4 – Parameters which varied between different times and days in kinetic model.

Parameter	10 June 08:35	10 June 12:35	10 June 16:35	10 June 20:35	8 June 17:35	19 June 17:35	25 June 17:35
AER (h^{-1})*	0.66	0.60	0.64	0.78	0.70	0.43	0.59
K_e (s^{-1})	10	3	10	5	3	3	1
$k_{aq,3}$ (cm^3 s^{-1})	2.9×10^{-18}	2.0×10^{-18}	1.3×10^{-18}	7.2×10^{-19}	5.0×10^{-18}	1.0×10^{-17}	5.0×10^{-18}
$k_{aq,14}$ (cm^3 s^{-1})	1.3×10^{-19}	6.3×10^{-20}	5.4×10^{-20}	5.4×10^{-20}	7.6×10^{-20}	2.5×10^{-19}	3.2×10^{-20}
$k_{aq,23}$ (cm^3 s^{-1})	1.5×10^{-4}	1.3×10^{-4}	8.7×10^{-5}	7.4×10^{-5}	2.6×10^{-4}	3.2×10^{-4}	2.4×10^{-4}
$k_{aq,24}$ (cm^3 s^{-1})	2.5	2.5	2.5	2	2	2	2.5
j_{Cl2} (s^{-1})**	2.2×10^{-4} /50	1.2×10^{-4}/50	3.4×10^{-4} /50	0	2.6×10^{-4} /50	2.6×10^{-4} /50	2.6×10^{-4} /50
j_{HOCl} (s^{-1})**	2.1×10^{-5} /50	1.1×10^{-5} /50	3.1×10^{-5} /50	0	2.4×10^{-5} /50	2.4×10^{-5} /50	2.4×10^{-5} /50

j_{ClNO2} (s^{-1})**	1.6×10^{-5} /50	8.2×10^{-6} /50	2.3×10^{-5} /50	0	1.7×10^{-5} /50	1.7×10^{-5} /50	1.7×10^{-5} /50
j_{NO2} (s^{-1})**	1.4×10^{-3} /50	7.5×10^{-4} /50	2.2×10^{-3} /50	0	1.7×10^{-3} /50	1.7×10^{-3} /50	1.7×10^{-3} /50
j_{NO3} (s^{-1})**	7.5×10^{-2} /50	2.3×10^{-2} /50	0.13 /50	0	0.11 /50	0.11 /50	0.11 /50
j_{HONO} (s^{-1})**	1.8×10^{-4} /50	1.0×10^{-4} /50	2.8×10^{-4} /50	0	2.1×10^{-4} /50	2.1×10^{-4} /50	2.1×10^{-4} /50
γ_{NO2}	0.08	0.08	0.08	0.08	0.08	0.04	0.06
$k_{s,44}$ (s^{-1})	2.0×10^{-3}	2.0×10^{-3}	2.0×10^{-3}	3.0×10^{-3}	4.0×10^{-3}	2.0×10^{-3}	1.0×10^{-3}
$k_{s,45}$ (s^{-1})	5.5×10^{-4}	4.4×10^{-4}	3.3×10^{-4}	2.5×10^{-4}	1.1×10^{-3}	2.2×10^{-4}	3.0×10^{-4}
$k_{s,46}$ (s^{-1})	8.3×10^{-4}	8.3×10^{-4}	8.3×10^{-4}	4.2×10^{-4}	8.3×10^{-4}	4.2×10^{-4}	4.2×10^{-4}
$k_{s,50}$ ($cm^3\ s^{-1}$)	1.0×10^{-16}	1.0×10^{-16}	1.0×10^{-16}	1.0×10^{-16}	1.0×10^{-16}	1.0×10^{-16}	1.0×10^{-15}
$k_{s,51}$ ($cm^3\ s^{-1}$)	1.0×10^{-15}	1.0×10^{-15}	1.0×10^{-15}	1.0×10^{-15}	1.0×10^{-15}	5.0×10^{-16}	1.0×10^{-15}
P_{NH3} ($cm^{-3}\ s^{-1}$) ***	$7.9 \times 10^{11} \times AER$	$6.4 \times 10^{11} \times AER$	$6.4 \times 10^{11} \times AER$	$1.7 \times 10^{11} \times AER$	$6.4 \times 10^{11} \times AER$	$9.8 \times 10^{11} \times AER$	$4.9 \times 10^{11} \times AER$
P_{NO2} ($cm^{-3}\ s^{-1}$) ***	$4.3 \times 10^{10} \times AER$	$4.3 \times 10^{10} \times AER$	$5.9 \times 10^{10} \times AER$	$8.3 \times 10^{10} \times AER$	$1.2 \times 10^{11} \times AER$	$2.2 \times 10^{11} \times AER$	$1.4 \times 10^{11} \times AER$
P_{NO} ($cm^{-3}\ s^{-1}$) ***	$4.2 \times 10^{10} \times AER$	$4.2 \times 10^{10} \times AER$	$3.9 \times 10^{10} \times AER$	$1.5 \times 10^{10} \times AER$	$3.5 \times 10^{10} \times AER$	$5.6 \times 10^{10} \times AER$	$5.0 \times 10^{10} \times AER$
P_{O3} ($cm^{-3}\ s^{-1}$) ***	$1.7 \times 10^{11} \times AER$	$1.7 \times 10^{11} \times AER$	$1.7 \times 10^{11} \times AER$	$1.7 \times 10^{11} \times AER$	$1.7 \times 10^{11} \times AER$	$1.7 \times 10^{11} \times AER$	$1.7 \times 10^{11} \times AER$
P_{HONO} ($cm^{-3}\ s^{-1}$) ***	$6.2 \times 10^{9} \times AER$	$6.2 \times 10^{9} \times AER$	$6.2 \times 10^{9} \times AER$	$6.2 \times 10^{9} \times AER$	$6.2 \times 10^{9} \times AER$	$1.4 \times 10^{10} \times AER$	$6.2 \times 10^{9} \times AER$
$P_{NO\_indoors}$ ($cm^{-3}\ s^{-1}$) ***	1.4×10^{7}	1.4×10^{7}	7.1×10^{6}	1.4×10^{7}	7.1×10^{6}	2.1×10^{7}	7.1×10^{6}
$P_{NO2\_indoors}$ ($cm^{-3}\ s^{-1}$) ***	2.1×10^{7}	2.1×10^{7}	3.6×10^{7}	5.0×10^{7}	5.0×10^{7}	2.1×10^{7}	7.1×10^{6}

* All species were removed from the gas-phase at the AER.

** Upper-bound photolysis rates from measurements were divided by a factor of 50.

*** P_X represents a production rate of molecules due to outdoor-to-indoor transport, while $P_{X\_indoors}$ represents an indoor production. P_{NH3}, P_{O3}, $P_{NO\_indoors}$ and $P_{NO2\_indoors}$ were fitting parameters while P_{NO2}, P_{NO} and P_{HONO} were based on measurements of these species outdoors. Note that P_{O3} was changed for the window opening scenarios. AER was in units of s^{-1}.

Table S5 – Outdoor mixing ratios and I^- TOF-CIMS instrumental detection limits for various bleach-related compounds during HOMEChem.

	Outdoor mixing ratio (pptv)				Detection limit (pptv)
	Median	*25th percentile*	*75th percentile*	*Mean (± S. D.)*	
HOCl	BDL	BDL	50.	40. ± 40.	30.
Cl_2	5.	BDL	11.	10. ± 10.	3.
$ClNO_2$	2.	BDL	7.	5. ± 7.	2.
$NHCl_2$*	BDL	BDL	BDL	BDL	1.
NCl_3*	BDL	BDL	0.2	0.2 ± 0.2	0.2
Cl_2O*	BDL	BDL	BDL	BDL	0.2
N_2O_5	--	--	--	--	1.

Outdoor measurements taken during bleach cleaning experiments on 8, 10, 19, and 25 June 2018. pptv = part-per-trillion by volume. BDL = below detection limit; S. D. = standard deviation. (*) denotes mixing ratios are estimates. (--) denotes missing data.

Table S6 – Kinetic model predictions of total OH radical production (%) from individual reaction mechanisms during bleach cleaning experiments at HOMEChem.

Reaction	10 June 08:35	10 June 12:35	10 June 16:35	10 June 20:35	8 June 17:35	19 June 17:35	25 June 17:35
HOCl + *hv* → OH + Cl	96.0	93.5	96.4	--	84.9	38.0	56.0
Cl + HO_2 → ClO + OH	0.0	0.0	0.0	--	0.0	0.0	0.0
HONO + hv → NO + OH	3.9	6.4	3.4	--	15.1	62.0	43.9
HO_2 + NO → OH + NO_2	0.2	0.2	0.2	--	0.0	0.0	0.2
HO_2 + O_3 → OH + $2O_2$	0.0	0.0	0.0	--	0.0	0.0	0.0

No OH radical production occurred at 20:35 on 10 June 2018 due to the absence of indoor photolysis reactions. (--) denotes missing data. Radical production was calculated between 0 and 2.5 hours after bleach cleaning.

Table S7 – Kinetic model predictions of total Cl radical production (%) from individual reaction mechanisms during bleach cleaning experiments at HOMEChem.

Reaction	10 June 08:35	10 June 12:35	10 June 16:35	10 June 20:35	8 June 17:35	19 June 17:35	25 June 17:35
Cl_2 + *hv* → 2Cl	81.0	79.5	83.6	--	68.6	65.6	70.9
HOCl + *hv* → OH + Cl	8.3	8.2	8.4	--	6.8	3.9	2.5
$ClNO_2$ + *hv* → NO_2 + Cl	0.5	0.6	0.4	--	0.9	2.0	1.0

$ClONO_2 + h\nu \rightarrow NO_3 + Cl$	0.0	0.0	0.1	--	0.0	0.0	0.0
$OH + HCl \rightarrow Cl + H_2O$	0.0	0.0	0.0	--	0.0	0.0	0.1
$OH + Cl_2 \rightarrow HOCl + Cl$	0.1	0.1	0.1	--	0.0	0.0	0.0
$OH + ClO \rightarrow HO_2 + Cl$	0.0	0.0	0.0	--	0.0	0.0	0.0
$ClO + NO \rightarrow Cl + NO_2$	10.0	11.6	7.3	--	23.7	28.4	25.4

No Cl radical production occurred at 20:35 on 10 June 2018 due to the absence of indoor photolysis reactions. (--) denotes missing data. Radical production was calculated between 0 and 2.5 hours after bleach cleaning.

References

(1) Farmer, D. K.; Vance, M. E.; Abbatt, J. P. D.; Abeleira, A.; Alves, M. R.; Arata, C.; Boedicker, E.; Bourne, S.; Cardoso-Saldaña, F.; Corsi, R.; DeCarlo, P. F.; Goldstein, A. H.; Grassian, V. H.; Hildebrandt Ruiz, L.; Jimenez, J. L.; Kahan, T. F.; Katz, E. F.; Mattila, J. M.; Nazaroff, W. W.; Novoselac, A.; O'Brien, R. E.; Or, V. W.; Patel, S.; Sankhyan, S.; Stevens, P. S.; Tian, Y.; Wade, M.; Wang, C.; Zhou, S.; Zhou, Y. Overview of HOMEChem: House Observations of Microbial and Environmental Chemistry. *Environ. Sci. Process. Impacts* **2019,** 10.1039/C9EM00228F.
(2) Zahniser, M.; Kaufman, F. Kinetics of the reactions of ClO with O and with NO. *J. Chem. Phys.* **1977,** *66* (8), 3673-3681.
(3) Xue, L.; Saunders, S.; Wang, T.; Gao, R.; Wang, X.; Zhang, Q.; Wang, W. Development of a chlorine chemistry module for the Master Chemical Mechanism. *Geosci. Model Dev.* **2015,** *8* (10), 3151-3162.
(4) Liu, Y.; Misztal, P.; Xiong, J.; Tian, Y.; Arata, C.; Nazaroff, W.; Goldstein, A. Detailed investigation of ventilation rates and airflow patterns in a northern California residence. *Indoor Air* **2018,** *28* (4), 572-584.
(5) Zhao, J.; Zhang, R. Proton transfer reaction rate constants between hydronium ion (H_3O^+) and volatile organic compounds. *Atmos. Environ.* **2004,** *38* (14), 2177-2185.
(6) Kowal, S. F.; Allen, S. R.; Kahan, T. F. Wavelength-Resolved Photon Fluxes of Indoor Light Sources: Implications for HOx Production. *Environ. Sci. Technol.* **2017,** *51* (18), 10423-10430.
(7) Aljawhary, D.; Lee, A.; Abbatt, J. High-resolution chemical ionization mass spectrometry (ToF-CIMS): application to study SOA composition and processing. *Atmos. Meas. Tech.* **2013,** *6* (11), 3211-3224.
(8) Lopez-Hilfiker, F. D.; Iyer, S.; Mohr, C.; Lee, B. H.; D'Ambro, E. L.; Kurten, T.; Thornton, J. A. Constraining the sensitivity of iodide adduct chemical ionization mass spectrometry to multifunctional organic molecules using the collision limit and thermodynamic stability of iodide ion adducts. *Atmos. Meas. Tech.* **2016,** *9* (4), 1505-1512.
(9) Bertram, T. H.; Kimmel, J. R.; Crisp, T. A.; Ryder, O. S.; Yatavelli, R. L. N.; Thornton, J. A.; Cubison, M. J.; Gonin, M.; Worsnop, D. R. A field-deployable, chemical ionization time-of-flight mass spectrometer. *Atmos. Meas. Tech.* **2011,** *4* (7), 1471-1479.
(10) Foster, K.; Caldwell, T.; Hemminger, J.; Finlayson-Pitts, B. Techniques for quantifying gaseous HOCl using atmospheric pressure ionization mass spectrometry. *Phys. Chem. Chem. Phys.* **1999,** *1* (24), 5615-5621.
(11) Lawler, M.; Sander, R.; Carpenter, L.; Lee, J.; Glasow, R. v.; Sommariva, R.; Saltzman, E. HOCl and Cl_2 observations in marine air. *Atmos. Chem. Phys.* **2011,** *11* (15), 7617-7628.
(12) Dubé, W. P.; Brown, S. S.; Osthoff, H. D.; Nunley, M. R.; Ciciora, S. J.; Paris, M. W.; McLaughlin, R. J.; Ravishankara, A. Aircraft instrument for simultaneous, in situ measurement of NO_3 and N_2O_5 via pulsed cavity ring-down spectroscopy. *Rev. Sci. Instrum.* **2006,** *77* (3), 034101.
(13) Fuchs, H.; Dubé, W. P.; Ciciora, S. J.; Brown, S. S. Determination of inlet transmission and conversion efficiencies for in situ measurements of the nocturnal nitrogen oxides, NO_3, N_2O_5 and NO_2, via pulsed cavity ring-down spectroscopy. *Anal. Chem.* **2008,** *80* (15), 6010-6017.
(14) Wagner, N.; Dubé, W.; Washenfelder, R.; Young, C.; Pollack, I.; Ryerson, T.; Brown, S. Diode laser-based cavity ring-down instrument for NO_3, N_2O_5, NO, NO_2 and O_3 from aircraft. *Atmos. Meas. Tech.* **2011,** *4* (6), 1227-1240.
(15) Leu, M.-T.; Timonen, R. S.; Keyser, L. F.; Yung, Y. L. Heterogeneous reactions of HNO_3(g) + NaCl(s) → HCl(g) + $NaNO_3$(s) and N_2O_5(g) + NaCl(s) → $ClNO_2$(g) + $NaNO_3$(s). *J. Phys. Chem.* **1995,** *99* (35), 13203-13212.
(16) Finlayson-Pitts, B. The tropospheric chemistry of sea salt: A molecular-level view of the chemistry of NaCl and NaBr. *Chem. Rev.* **2003,** *103* (12), 4801-4822.

(17) Lee, B. H.; Lopez-Hilfiker, F. D.; Mohr, C.; Kurten, T.; Worsnop, D. R.; Thornton, J. A. An iodide-adduct high-resolution time-of-flight chemical-ionization mass spectrometer: application to atmospheric inorganic and organic compounds. *Environ. Sci. Technol.* **2014,** *48* (11), 6309-17.
(18) Kercher, J.; Riedel, T.; Thornton, J. Chlorine activation by N_2O_5: simultaneous, in situ detection of $ClNO_2$ and N_2O_5 by chemical ionization mass spectrometry. *Atmos. Meas. Tech.* **2009,** *2* (1), 193-204.
(19) Brophy, P.; Farmer, D. K. Clustering, methodology, and mechanistic insights into acetate chemical ionization using high-resolution time-of-flight mass spectrometry. *Atmos. Meas. Tech.* **2016,** *9* (8), 3969-3986.
(20) Iyer, S.; Lopez-Hilfiker, F.; Lee, B. H.; Thornton, J. A.; Kurtén, T. Modeling the detection of organic and inorganic compounds using iodide-based chemical ionization. *J. Phys. Chem. A* **2016,** *120* (4), 576-587.
(21) Huey, L. G.; Hanson, D. R.; Howard, C. J. Reactions of SF_6^- and I^- with atmospheric trace gases. *J. Phys. Chem.* **1995,** *99* (14), 5001-5008.
(22) Wong, J.; Carslaw, N.; Zhao, R.; Zhou, S.; Abbatt, J. Observations and impacts of bleach washing on indoor chlorine chemistry. *Indoor Air* **2017,** *27* (6), 1082-1090.
(23) Jafvert, C. T.; Valentine, R. L. Reaction scheme for the chlorination of ammoniacal water. *Environ. Sci. Technol.* **1992,** *26* (3), 577-586.
(24) Deborde, M.; Von Gunten, U. Reactions of chlorine with inorganic and organic compounds during water treatment—kinetics and mechanisms: a critical review. *Water Res.* **2008,** *42* (1-2), 13-51.
(25) Eiserich, J. P.; Cross, C. E.; Jones, A. D.; Halliwell, B.; Van der Vliet, A. Formation of nitrating and chlorinating species by reaction of nitrite with hypochlorous acid a novel mechanism for nitric oxide-mediated protein modification. *J. Biol. Chem.* **1996,** *271* (32), 19199-19208.
(26) Frenzel, A.; Scheer, V.; Sikorski, R.; George, C.; Behnke, W.; Zetzsch, C. Heterogeneous interconversion reactions of $BrNO_2$, $ClNO_2$, Br_2, and Cl_2. *J. Phys. Chem. A* **1998,** *102* (8), 1329-1337.
(27) Atkinson, R.; Baulch, D. L.; Cox, R. A.; Crowley, J. N.; Hampson, R. F.; Hynes, R. G.; Jenkin, M. E.; Rossi, M. J.; Troe, J. Evaluated kinetic and photochemical data for atmospheric chemistry: Volume I - gas phase reactions of O_x, HO_x, NO_x and SO_x species. *Atmos. Chem. Phys.* **2004,** *4* (6), 1461-1738.
(28) Wilkins Jr, R. A.; Hisatsune, I. The reaction of dinitrogen pentoxide with hydrogen chloride. *Ind. Eng. Chem. Fundam.* **1976,** *15* (4), 246-248.
(29) George, I.; Matthews, P.; Whalley, L.; Brooks, B.; Goddard, A.; Baeza-Romero, M.; Heard, D. Measurements of uptake coefficients for heterogeneous loss of HO_2 onto submicron inorganic salt aerosols. *Phys. Chem. Chem. Phys.* **2013,** *15* (31), 12829-12845.
(30) Cook, J. E. L.; Ennis, C. A.; Leck, T. J.; Birks, J. W. Studies of reactions of importance in the stratosphere. IV. Rate constant for the reaction Cl+HOCl→HCl+ClO over the temperature range 243–365 K. *J. Chem. Phys.* **1981,** *74* (1), 545-549.
(31) Sander, R. Compilation of Henry's law constants (version 4.0) for water as solvent. *Atmos. Chem. Phys.* **2015,** *15* (8), 4399-4981.
(32) Shi, Q.; Jayne, J.; Kolb, C.; Worsnop, D.; Davidovits, P. Kinetic model for reaction of $ClONO_2$ with H_2O and HCl and HOCl with HCl in sulfuric acid solutions. *J. Geophys. Res. Atmos.* **2001,** *106* (D20), 24259-24274.
(33) Tang, M.; Cox, R.; Kalberer, M. Compilation and evaluation of gas phase diffusion coefficients of reactive trace gases in the atmosphere: volume 1. Inorganic compounds. *Atmos. Chem. Phys.* **2014,** *14* (17), 9233-9247.(1) Abdullahi, K. L.; Delgado-Saborit, J. M.; Harrison, R. M. Emissions and indoor concentrations of particulate matter and its specific chemical components from cooking: A review. *Atmos. Environ.* **2013,** *71*, 260-294.
(34) Abdullahi, K. L.; Delgado-Saborit, J. M.; Harrison, R. M. Emissions and indoor concentrations of particulate matter and its specific chemical components from cooking: A review. *Atmos. Environ.* **2013,** *71*, 260-294.

(35) Xu, W.; Lambe, A.; Silva, P.; Hu, W.; Onasch, T.; Williams, L.; Croteau, P.; Zhang, X.; Renbaum-Wolff, L.; Fortner, E. Laboratory evaluation of species-dependent relative ionization efficiencies in the Aerodyne Aerosol Mass Spectrometer. *Aerosol Sci. Technol.* **2018,** *52* (6), 626-641.